

Article

Smart Sensors System Based on Smartphones and Methodology for 3D Modelling in Shallow Water Scenarios

Gabriele Vozza ^{1,*}, Domenica Costantino ¹ , Massimiliano Pepe ²  and Vincenzo Saverio Alfio ¹ 

¹ Dipartimento di Ingegneria Civile, Ambientale, del Territorio, Edile e di Chimica, Polytechnic University of Bari, Via E. Orabona 4, 70125 Bari, Italy

² Department of Engineering and Geology (InGeo), “G. d’Annunzio” University of Chieti-Pescara, Viale Pin-Daro 42, 65127 Pescara, Italy

* Correspondence: gabriele.vozza@poliba.it

Abstract: The aim of the paper was the implementation of low-cost smart sensors for the collection of bathymetric data in shallow water and the development of a 3D modelling methodology for the reconstruction of natural and artificial aquatic scenarios. To achieve the aim, a system called GNSS > Sonar > Phone System (G > S > P Sys) was implemented to synchronise sonar sensors (Deeper Smart Sonars CHIRP+ and Pro+ 2) with an external GNSS receiver (SimpleRTK2B) via smartphone. The bathymetric data collection performances of the G > S > P Sys and the Deeper Smart Sonars were studied through specific tests. Finally, a data-driven method based on a machine learning approach to mapping was developed for the 3D modelling of the bathymetric data produced by the G > S > P Sys. The developed 3D modelling method proved to be flexible, easily implementable and capable of producing models of natural surfaces and submerged artificial structures with centimetre accuracy and precision.

Keywords: smartphone; smart sensors; bathymetry; machine learning; 3D modelling



Citation: Vozza, G.; Costantino, D.; Pepe, M.; Alfio, V.S. Smart Sensors System Based on Smartphones and Methodology for 3D Modelling in Shallow Water Scenarios. *Appl. Syst. Innov.* **2023**, *6*, 28. <https://doi.org/10.3390/asi6010028>

Academic Editor: Friedhelm Schwenker

Received: 9 January 2023

Revised: 25 January 2023

Accepted: 8 February 2023

Published: 10 February 2023



Copyright: © 2023 by the authors. Licensee MDPI, Basel, Switzerland. This article is an open access article distributed under the terms and conditions of the Creative Commons Attribution (CC BY) license (<https://creativecommons.org/licenses/by/4.0/>).

1. Introduction

In September 2015, the 2030 Agenda for Sustainable Development was signed by 193 United Nations (UN) countries. Specifically, the 14th goal (Life below water) is dedicated to: “Conserve and sustainably use the oceans, seas and marine resources for sustainable development”. In the targets defined by the 2030 Agenda to reach goal 14, the target 14.a aims to: “Increase scientific knowledge, develop research capacity and transfer marine technology, taking into account the Intergovernmental Oceanographic Commission Criteria and Guidelines on the Transfer of Marine Technology, in order to improve ocean health and to enhance the contribution of marine biodiversity to the development of developing countries, in particular small island developing States and least developed countries” [1]. Furthermore, 2021–2030 was declared by the United Nations as the “Decade of Ocean Science for Sustainable Development” and among the social outcomes to be achieved is “Data Transparency and Accessibility”, which aims to achieve an ocean with open access to data, information and technologies for nations, stakeholders and citizens [2].

Unfortunately, obtaining data and information from underwater environments with proprietary instrumentation is often difficult. In particular, bathymetric data, which are the subject of this work, are expensive data in terms of instrumentation, specialised staff, logistics, time and mode of execution [3–6]. These elements may be an obstacle to achieving the sustainability goals of the 2030 Agenda and the Decade of the Ocean. However, the emergence in the consumer market of new smart and Internet of Things (IoT) technologies for mapping aquatic and marine environments is an opportunity to disseminate low-cost instrumentation for research purposes, democratisation and access to data even in remote areas, and involvement of the population in citizen science projects.

For these reasons, this paper intends to investigate the Single Beam Echo Sounders (SBES) sonar (SOund Navigation And Ranging) produced by Deeper UAB. These SBES, called Deeper Smart Sonar, are inexpensive, lightweight devices that are easy to use even by non-experts, can be mounted on Unmanned Aerial Vehicles (UAVs)/Unmanned Surface Vehicles (USVs) and, as will be seen in the literature review section, found some interest in scientific applications.

1.1. Literature Review

Concerning the use of Deeper Smart Sonar in science, Bandini et al. [7] used the Deeper Smart Sonar Pro+ connected to a UAV via a winch to survey three inland water bodies in Denmark: Lake Furesø, Marrebæk Kanal and Åmose Å. The authors estimated that the Global Navigation Satellite System (GNSS) receiver built into the Deeper Smart Sonar Pro+ had an accuracy of several metres (up to 30) and, through comparison with sample depth measurements, that the sonar committed an error of 3.8%. Bandini et al. [7] then proposed a method of correcting the horizontal positioning of the SBES using the nadiral images acquired by a UAV equipped with GNSS, Inertial Measurement Unit (IMU) and RADAR sensors, while the depth was corrected by linear regression with ground truths collected during the survey. After applying these methods, the authors obtained a horizontal positioning accuracy of about 20 cm and an error of about 2.1% for depths up to about 30 metres.

Alvarez et al. [8], through the integration of UAV imagery, sonar (data from the Deeper Smart Sonar Pro+) and adaptive sampling, surveyed a small reservoir located at the Kessler Atmospheric and Ecological Field Station (KAEFS) near Purcell, Oklahoma, USA. In order to perform the survey, the authors connected the SBES to a UAV via a cable and a small vessel containing an Android tablet to collect bathymetric data. Alvarez et al. (2018), comparing the direct measurements with echosounder measurements, observed a Root Mean Square Error (RMSE) of 0.0147 and an R of 0.987.

Giambastiani et al. [9] used the Deeper Smart Sonar Pro+, connected to a bait boat, to collect depth measurements of small-to-medium water bodies (between 50,000 and 2000 square metres) located in Tuscany. The authors described the sonar's internal GNSS as "highly accurate". From the acquired data, the authors deduced the volume of the water bodies investigated (204) and found a high correlation ($R^2 = 94$) between the deduced volumes and the actual volumes of some sampled water bodies (55).

Bogoyavlensky et al. [10] by combining data from UAVs, georadar and two sonars, one of them a Deeper Smart Sonar Pro+, surveyed the Seyakha C11 crater in Siberia and produced a Digital Elevation Model (DEM) of it. The Deeper Smart Sonar Pro+ was geolocated with the internal GNSS and the authors reported a positioning accuracy of up to 3 metres.

Kellerer-Pirklbauer et al. [11] used the Deeper Smart Sonar CHIRP+ (technological successor of the Pro+) with other sensors to study the recession processes of the Pasterze glacier in Austria. Using the CHIRP+, the authors highlighted that there was a lack of reference studies on the CHIRP+ that indicated the accuracy of SBES in measuring depth. However, the authors estimated the accuracy of water depth measurements of less than 0.1 m in shallow waters (<5 m) and flat bottoms, and 0.5 m for deeper waters with sloping bottoms.

Broere et al. [12] used the Deeper Smart Sonar CHIRP+ to detect suspended macro-plastics in rivers. The authors demonstrated with this research that they could detect suspended macro-plastics with low-cost sonar and that specific plastic objects had different reflections.

Ruffell et al. [13] tested a system called "Dronar" for forensic purposes. The system consisted of a Deeper Smart Sonar (Pro+ or CHIRP+ 2) connected by wire to a UAV. The authors showed how the Dronar could be a system to identify sunken objects, provide background information for further investigation and signal possible dangers to the navigation of boats and divers.

Sanjou et al. [14] developed a floating UAV system for measuring natural river discharge. The system consisted of a UAV equipped with a floating ring, a Global Positioning System-Real-Time Kinematic (GPS-RTK) receiver (DG-PRO1RWS) a smartphone for data recording and a Deeper Smart Sonar Pro+. By combining the GPS-RTK receiver to measure the river's velocity and the sonar to take cross-sections, the authors were able to derive the discharge of the river.

Koutalakis et al. [15] created a UAV + sonar system to estimate the velocity and discharge of a river using images collected by the UAV (IV-UAV) and bathymetry detected using the Deeper Smart Sonar Pro+.

In a research work, Bandini et al. [16] focused on the use of Ground Penetrating Radar (GPR) and Unmanned Aerial Systems (UAS) for mapping inland water bodies, and posed the question of applying GNSS Post-Processed Kinematic (PPK) corrections to the Deeper Smart Sonar CHIRP+ to improve geolocation. In this latter paper, the authors logged separately on a BeagleBone Black single-board computer the sonar data in NMEA0183 format and the GNSS raw data from a ZED-F9P receiver during the bathymetric survey. In post-processing, the authors, based on Coordinated Universal Time (UTC) timestamps, matched the sonar data with the GNSS positioning data processed in PPK to re-estimate the sonar position.

1.2. Aim of the Paper

The analysis of the state of art revealed discordant values regarding the achievable accuracy of this type of sensor for bathymetry. Therefore, the lack of these data makes it difficult to frame the surveys conducted in more general scenarios and thus define application ranges with some geomatics sensibility. Based on these considerations, this paper proposes to analyse the following aspects:

1. Tests to determine the accuracy and precision of shallow-water depth measurement and planimetric positioning of Deeper Smart Sonar (particularly CHIRP+ and Pro+ 2), implementation and evaluation of a system to synchronise the Deeper Smart Sonars with an external GNSS receiver via smartphone to improve the GNSS Single Point Positioning (SPP) performance in real-time, and a method to correct the GNSS positioning of the Deeper Smart Sonar in Post-Processed Kinematic (PPK) based on a spacetime approach and on the GPS Time (GPST) to further optimise positioning performance;
2. Building 3D mesh models of the environments surveyed with the Deeper Smart Sonar.

In order to make a comparison with internationally accepted reference values, data collected during the tests and the aims achieved in the research were analysed first taking into consideration the standardised uncertainty values of the International Hydrographic Organization (IHO) [17] and then considering possible applications in science and engineering fields.

2. Materials and Methods

2.1. Research Methodology

To achieve the aims enunciated in Section 1.2, the research was divided into three phases.

In the first phase an electronic system was implemented to synchronise the Deeper Smart Sonar CHIRP+ or Pro+ 2 and an external GNSS receiver (SimpleRTK2B) via smartphone, the system was called GNSS > Sonar > Phone System (G > S > P Sys). The idea behind the implementation of the G > S > P Sys was to create a network for data exchange, using the smartphone as a platform for input and output data management between the external GNSS receiver and the sonar. The final aim of the System was to send real-time SPP positioning data from the external GNSS receiver to the Deeper Smart Sonar. The System improves sonar geolocation during the bathymetric survey and simultaneously records the raw data from the external GNSS receiver for post-processing in PPK, to additionally improve the sonar GNSS positioning in post-processing. The real-time correction of sonar geolocation via an external GNSS receiver was possible due to the "mock location" function

present in Android smartphones. Using this function, an app connected to an external GNSS receiver can correct the geolocation of other apps on the smartphone.

In the second phase, through some specific tests, several datasets were built to study the performance of the Deeper Smart Sonar and G > S > P Sys. A preliminary test was performed to evaluate the performance in static GNSS positioning of the Deeper Smart Sonar (CHIRP+ and Pro+ 2) and the G > S > P Sys. Subsequently, two tests were performed under dynamic conditions to evaluate the performance of the Deeper Smart Sonars and the G > S > P Sys in kinematic positioning. To study the accuracy and precision of the Deeper Smart Sonars in measuring water depth, a test under controlled conditions in a swimming pool and a test under real conditions in the sea were performed.

In order to apply the PPK correction method of sonar geolocation and test the pipeline for 3D modelling of the data obtained from the G > S > P Sys, the complete survey of a swimming pool and the survey of a portion of the seabed was performed.

Based on the pool survey, a dataset was created to test the 3D modelling of artificial structures, while based on the sea survey, a dataset was created to test the 3D modelling of natural surfaces. In addition, the purpose of the sea test was also to analyse the devices under real operating conditions. Both tests were performed using the Deeper Smart Sonar CHIRP+.

In the third research phase, a pipeline was created for the 3D modelling of natural surfaces and artificial structures. The 3D modelling method used can be classified in the macro-group of data-driven modelling [18].

The pipeline developed for modelling natural surfaces consists of three steps: synchronisation, interpolation and 3D modelling.

In the synchronisation step, the GNSS positions recorded by the external receiver and corrected in PPK were synchronised with the depth values recorded by the sonar; the sonar GNSS position was corrected during the survey.

The proposed method is spatio-temporal as it is performed by synchronising the data produced by the System first based on latitude and longitude coordinates and then on the GPS Time (GPST). This step is possible because, through the electronic synchronisation in real-time of the devices via smartphone, the external GNSS receiver previously transmitted its coordinates to the sonar. The operation allows synchronisation to a one thousandth of a second ($1/1000$).

The interpolation step was performed in order to transform isolated data into continuous data in a grid format. To generate the bathymetric grid, an innovative interpolation method based on Machine Learning (ML) was used. In particular, the Forest-based Classification and Regression algorithm implemented in ArcGIS PRO software (ESRI, Redlands, CA, USA) was applied. This algorithm is a powerful classification and regression method based on the Random Forest supervised ML method of Leo Breiman and Adele Cutler.

In the most general form, proposed by Leo Breiman [19], a Random Forest for regression generates trees that grow according to a random vector Θ . The tree predictor $h(x, \Theta)$ takes numerical values and the training set is assumed to be independently extracted from the random vector Y, X . The mean-squared generalization error for any predictor $h(x)$ is:

$$E_{X,Y}(Y - h(X))^2 \quad (1)$$

In order to use only the detected bathymetric data, without external data (e.g., satellite images), a grid produced by the Inverse Distance Weight (IDW) method was used to define the initial training features of the algorithm [20,21].

The formula used for the IDW interpolation was [22,23]:

$$V_g = \frac{\sum_{i=1}^n \frac{v_i}{d_i^p}}{\sum_{i=1}^n \frac{1}{d_i^p}} \quad (2)$$

where:

V_g : value of the point to be estimated at the x and y coordinates of the grid;
 v_i : value of the i -th observed point;
 n : number of points close to the point to be interpolated;
 d_i : distance of the i -th point from the point to be interpolated;
 P : a positive parameter representing power.

The grid IDW was subsequently transformed into a 3D model to be used for comparative purposes in the results analysis process.

In order to be able to make a subsequent comparison with the 3D model (generated on the basis of the grid produced with Forest-based Classification and Regression) an additional grid was generated in ArcGIS Pro using the Ordinary Kriging interpolation method.

In the Kriging method, the spatial correlation between the surveyed points can be estimated using [24,25]:

$$\hat{\gamma}(d) = \frac{1}{2|N(d)|} \sum_{N(d)} [V(u_i) - V(u_j)]^2 \tag{3}$$

where:

$N(d)$: set of pairs of measured points;

$|N(d)|$: number of distinct pairs in $N(d)$;

d : separation vector between points;

$|d|$: equal to $u_i - u_j$;

$V(u_i)$: value of the random variable to describe the possible outcomes of the measured quantity V in the spatial location u_i ;

$V(u_j)$: value of the random variable to describe the possible outcomes of the quantity V in the spatial location u_j .

This method was chosen as it emerges in the literature as one of the best and most flexible interpolation methods, which is also valid for the interpolation of bathymetric data [26].

Finally, in the 3D modelling phase, the three bathymetric grids produced (with Forest-based Classification and Regression, Ordinary Kriging and IDW) were transformed into 3D triangular mesh models. The idea behind the transformation consists in the possibility of interpreting the bathymetric grids as a set of digital values in matrix form. Based on this principle, bathymetric grids were first transformed into point clouds and subsequently modelled in 3D. The 3D modelling was performed by applying the Poisson surface reconstruction method. The Poisson method, given a set S of points p of a solid model M whose surface area is ∂M , reconstructs the 3D surface area by solving a classical Poisson problem [27,28]:

$$\Delta \tilde{X} = \nabla \cdot \vec{V} \tag{4}$$

with \vec{V} vector field. The gradient of the smoothed indicator function of M is equal to the vector field obtained by smoothing the field normal to the surface:

$$\nabla (X_M * \tilde{F})(q_0) = \int_{\partial M} \tilde{F}_p(q_0) \vec{N}_{\partial M}(p) dp \tag{5}$$

where:

$\vec{N}_{\partial M}$: normal to the surface of point p ;

\tilde{F} : smoothing filter.

The integral cannot be solved directly since the surface of the solid to be modelled is not known.

To solve the problem, using the set of points p , the surface is divided into many patches and the integral on a patch is approximated to the value of the point, scaled by the area of the patch:

$$\nabla(X_M * \tilde{F})(q) = \sum_{s \in S} \int_{P_s} \tilde{F}_p(q) \vec{N}_{\partial M}(p) dp \approx \sum_{s \in S} |P_s| \tilde{F}_{s,p}(q) s \cdot \vec{N} \equiv \vec{V}(q) \quad (6)$$

The modelling of artificial structures was treated as a special case of the modelling of natural surfaces and the pipeline is theoretically not different from the one just described.

Section 2.4.4 was dedicated specifically to the modelling of artificial structures; indeed, in this section, it is possible to find further information and a description of how the pipeline was implemented.

2.2. GNSS > Sonar > Phone System Implementation

2.2.1. Devices and Apps

The G > S > P Sys consists of a hardware part and a software part. The hardware components forming the G > S > P Sys and tested, also individually, in this work were the Deeper Smart Sonar Pro+ 2 (Deeper UAB, Vilnius, Lithuania), the Deeper Smart Sonar CHIRP+ (Deeper UAB, Vilnius, Lithuania), the SimpleRTK2B (ArduSimple, Principality of Andorra) and the Huawei P30 Pro (Huawei Technologies Co., Ltd., Shenzhen, China).

The Deeper Smart Sonar Pro+ 2 and CHIRP+ are two Single Beam Echo Sounders [29,30] operating at frequencies of 100 kHz, 240 kHz and 675 kHz and with scan cones of 47°, 20° and 7° respectively. The devices perform about 15 scans per second and cover a depth ranging from a minimum of 0.15 m to a maximum of 100 m.

The Deeper Smart Sonars have an internal GNSS receiver that enables geolocation. Alternatively, they can geolocate themselves via the GNSS receiver of the smartphone. The Sonars connect to the smartphone via Wi-Fi and are controlled by an app called Fish Deeper—Fishing App. This allows Sonars to transmit their data to the smartphone (Sonar data in Figure 1).

Due to geolocation, the Sonars produce 2D maps with the bathymetric information obtained while scanning the bottom. The products of a survey immediately available to a user consist of a georeferenced sonar scan of the bottom and a 2D bathymetric map. The products are displayed in real-time on the smartphone and, after the survey, are also available via the web platform of Deeper UAB. Instead, the raw data, downloadable from the smartphone and the web platform, consist of a text file (*.csv) containing the latitude and longitude of the acquired points, the depth values recorded from the bottom scans (in metres), the water temperature values (in °C) and the acquisition time of the sonar scans (in UNIX format).

The difference between the Deeper Smart Sonar CHIRP+ and the Pro+ 2 consists of the CHIRP technology. CHIRP stands for “Compressed High Intensity Radar Pulse” and sonar with CHIRP technology, unlike a classic sonar, scans the bottom by sending multiple pulses simultaneously.

This provides more information and allows it to create more accurate scans, better detect the bottom and better separate targets.

Table 1 shows the technical features of the Deeper Smart Sonar Pro+ 2 and the Deeper Smart Sonar CHIRP+.

Table 1. Technical features of the Deeper Smart Sonar Pro+ 2 and the Deeper Smart Sonar CHIRP+.

Device	Deeper Smart Sonar Pro+ 2	Deeper Smart Sonar CHIRP+
Image		
Beam cone	47°-20°-7°	47°-20°-7°
Frequency	100-240-675 kHz	100-240-675 kHz
GNSS	GPS, GLONASS, Galileo, BeiDou, QZSS	GPS, GLONASS, Galileo, BeiDou, QZSS
Wi-Fi connection range	100 m	100 m
Sonar scan rate	15x/s	15x/s
Depth range min/max	0.15–100 m	0.15–100 m
Weight	90 g	90 g
Dimensions	Ø 65 mm	Ø 65 mm
Operating temperature	−20 °C/40 °C	−20 °C/40 °C

The SimpleRTK2B is an external GNSS receiver based on the ZED-F9P GNSS module made by U-Blox (U-Blox, Thalwil, canton of Zürich, Switzerland) that can be connected to various devices including smartphones allowing more precise geolocation [31]. The SimpleRTK2B allows observation of GPS, GLONASS, Galileo and Beidou constellations and reception of the L1C/A L2C, L1OF L2OF, E1-B/C E5b, B1I B2I frequencies. In this work, a Bluetooth data transmission module (AS-XBEE-BT-2.4-INT-00) and a Helical multiband GNSS antenna (IP67) were added to the receiver. Using U-Center (software to manage U-Blox GNSS), the receiver was programmed to transmit via Bluetooth the real-time position in Single Point Positioning (GNSS-SPP data Real-time in Figure 1) and transmit via USB On-The-Go (USB OTG) connection the GNSS raw data in *.ubx format (GNSS-Raw data in Figure 1). Two files were produced from the file containing the GNSS raw data (in *.ubx format): the first file was produced via U-center (in *.csv format) and contained mainly the coordinates of latitude and longitude, ellipsoid height and GPS Time of the positioning performed by the device in SPP in real time; the second file was produced with RTKLIB: demo5_b34f.1 (version of RTKLIB [32] developed by rtklibexplorer [33] for working with the ZED-F9P and downloadable from <https://github.com/rtklibexplorer/RTKLIB/releases/tag/b34f> (accessed on 8 January 2023)) and consisted of a RINEX (Receiver INdependent EXchange) file of the observables for subsequent post-processing. The post-processed file mainly contained latitude, longitude, ellipsoidal height and GPS Time. Table 2 shows the technical features of the SimpleRTK2B.

Table 2. Technical features of the SimpleRTK2B.

Device	SimpleRTK2B
Image	
GNSS Module	ZED-F9P
Constellation	GPS, GLONASS, Galileo, Beidou
Frequency	L1C/A L2C, L1OF L2OF, E1-B/C E5b, B1I B2I
Bluetooth connection module	AS-XBEE-BT-2.4-INT-00
Antenna	Lightweight helical for multiband GNSS (IP67)
Weight	20 g
Dimensions	69 × 53 mm

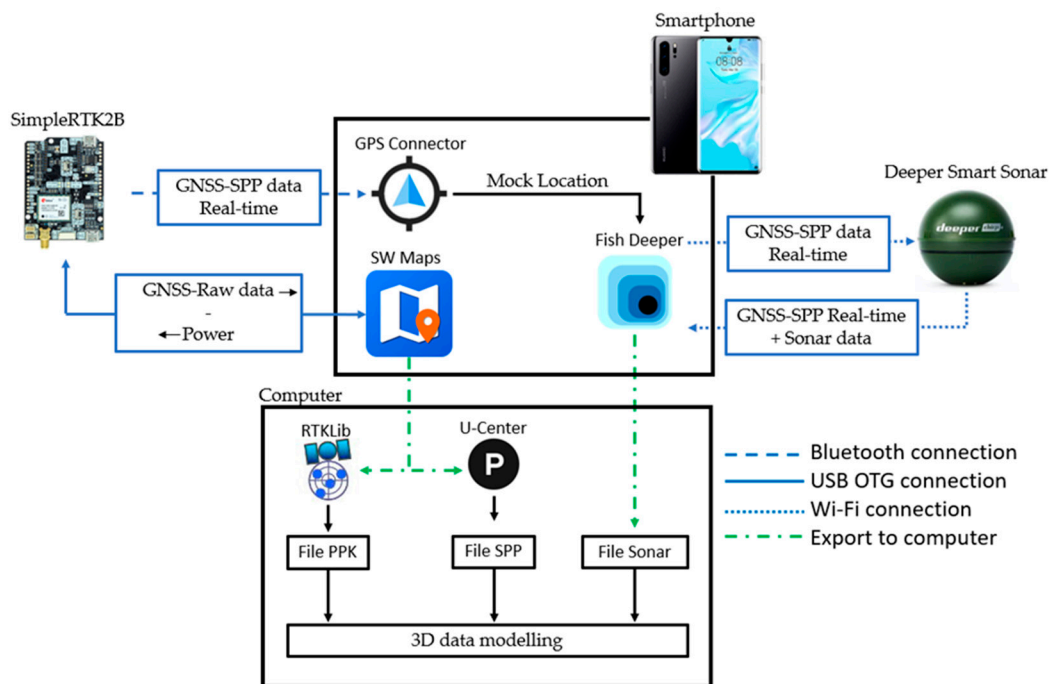


Figure 1. Synthetic pipeline of the $G > S > P$ Sys functioning.

In this case study, a Huawei P30 Pro smartphone was used to synchronise the Deeper Smart Sonars and the SimpleRTK2B. For the implementation of the $G > S > P$ Sys, the model of the smartphone is not particularly relevant. However, it is important that the smartphone has a good chipset and good RAM (Random Access Memory) to manage several apps at the same time in the background, an Android OS, the possibility of activating the “mock location” and finally the possibility of receiving data via USB OTG connection. The Huawei P30 Pro matches these features, it has a Huawei HiSilicon Kirin 980 chipset, 8 GB of RAM, the EMUI 12.0 OS, USB OTG connection and “mock location”.

The apps constituting the software part were: GPS Connector v1.0.1.7 (PilaBlu -Apps, Stuttgart, Germany), SW Maps GIS & Data Collector v2.9.1.1 (Softwel Pvt. Ltd., Kathmandu, Nepal) and Fish Deeper—Fishing App v1.22.0.3259 (Deeper UAB, Vilnius, Lithuania).

GPS Connector (developed by PilaBlu) allows an external GNSS receiver to be connected to the smartphone via Bluetooth or a USB connection. GPS Connector provides the external GNSS position data to other apps that use navigation data on the smartphone via the “mock location” and consequently improves the GNSS positioning performance of the other apps on the device. The app was used to improve the real-time SPP positioning of the Fish Deeper—Fishing App and consequently the sonar. For this app Android 4.1 or later is required.

SW Maps (developed by Softwel) has many functions related to the world of GIS (Geographic Information System) and allows an external GNSS receiver to be connected to the smartphone via Bluetooth or USB. This app was used to record data from the connected external GNSS receiver in *.ubx format for post-processing. SW Maps requires Android 4.4 or later.

Fish Deeper—Fishing App (developed by Deeper UAB) connects the Deeper Smart Sonars to the smartphone via Wi-Fi and allows the user to set the sonar scanning parameters (e.g., beam scan angles or fishing mode: Onshore, Boat, Ice fishing, Bait Boat and Scan Only), view the surveyed data (temperature, water depth, bathymetric map and sonar scan) and download the raw data [34]. The app requires Android 7.0 or later.

2.2.2. Connection Management and App Data Transfer

In order to make the operating system and synchronise the devices described, the connections of devices and the transmission of data between apps must be organised correctly.

The external GNSS receiver (SimpleRTK2B) was connected via USB OTG connection to the smartphone to receive power from the smartphone and transmit the GNSS-Raw data to the SW Maps app, which recorded the GNSS-Raw data for post-processing (GNSS-Raw data—Power in Figure 1). Simultaneously, the external GNSS receiver was connected via Bluetooth to the smartphone in order to transmit in real-time the GNSS SPP positioning data (GNSS-SPP data Real-time in Figure 1) to the GPS Connector app. The GPS Connector re-transmits the GNSS-SPP data Real-time to the Fish Deeper—Fishing App using the “mock location” function of the smartphone. Finally, the Deeper Smart Sonar was connected to the smartphone via Wi-Fi to receive the GNSS-SPP data Real-time by the Fish Deeper—Fishing App and re-transmit the GNSS-SPP data Real-time and the Sonar data to the Fish Deeper—Fishing App (GNSS-SPP Real-time + Sonar data Figure 1).

In order to allow GPS Connector to send external GNSS positioning data to other apps, GPS Connector must be enabled via the “mock location” function accessible from the developer options (developer options must be unlocked depending on the type of smartphone) and via the settings of the app itself. This step is very important as it allows the real-time synchronisation between the external GNSS receiver and sonar and the subsequent synchronisation in PPK.

To enable the sonar to geolocate itself via GNSS data received from the smartphone in the Fish Deeper—Fishing App, “Boat” must be selected as the fishing mode. In addition, to improve the connection between the smartphone and the sonar, Deeper UAB recommends disabling the mobile data and the settings that automatically switch between Wi-Fi and mobile data to stay online. Therefore, internet access is not available during the survey. Finally, during the experimentation with the Huawei P30 Pro, it was noted that in order to prevent GNSS positioning from being compromised by mobile and Wi-Fi networks surrounding the area to be surveyed, it would be advisable to disable the “Google Location Accuracy—Improve Location Accuracy” function; we do not know if this problem is also present on other smartphones.

2.3. Tests and Datasets Creation

The following sections describe the tests performed and the datasets constructed to analyse the performance of the devices investigated.

During the tests, sonar scans were performed at a frequency of 675 kHz and a 7° cone, the frequency was chosen as the most accurate to operate in the test scenarios [16]. Post-processing for relative GNSS positioning was performed with the HxGN SmartNet permanent station network (Hexagon AB, Stockholm, Sweden), the closest station was TARA located on the roof of the Polytechnic University of Bari, Taranto, Italy. The software used for the static and kinematic post-processing was primarily RTKLIB: demo5_b34f.1, while the post-processing in Precise Point Positioning (PPP) was performed with CSRS-PPP [35,36].

2.3.1. Static Datasets

The preliminary test to study the performance of the static GNSS positioning of the Deeper Smart Sonar Pro+ 2 and CHIRP+ and the G > S > P Sys was performed in Open Sky conditions on the roof of the Polytechnic University of Bari, Taranto, Italy, site of the Geomatics Laboratory in Taranto. To perform the test, the instrumentation was placed on an old vertex of a permanent GNSS network, named FATA which was already used in previous experiments [36]. For greater accuracy, the vertex coordinates were re-acquisition by the professional GNSS receiver Trimble R10. The Deeper Smart Sonars were placed on the observation vertex using a cylindrical vessel approximately 0.25 m high, filled with water (to turn on the sonars and guarantee the recording of GNSS data), with a hole at the

top equal to the diameter of the sonar to allow the sonars to be centred. The G > S > P Sys was positioned by installing the Helical antenna on the point to be surveyed using a stand. Each device conducted 8 h (28,800 s) of static observation and five datasets were produced. Two datasets were built with the real-time planimetric GNSS positioning in SPP, from the Deeper Smart Sonar CHIRP+ and the Deeper Smart Sonar Pro+ 2. One dataset was built with the real-time 3D GNSS positioning in SPP, from the G > S > P Sys. Another dataset was created with post-processed data in PPP 3D static, from the G > S > P Sys, and finally, one dataset post-processed in 3D static positioning was created from the G > S > P Sys. Table 3 shows the composition of the static datasets, “Deeper GNSS CHIRP+ ” refers to the internal GNSS receiver of the Deeper Smart Sonar CHIRP+ and “Deeper GNSS Pro+ 2” refers to the internal GNSS receiver of the Deeper Smart Sonar Pro+ 2.

Table 3. Static datasets composition.

Device	Positioning	Obs. Time (s)	Data Sample (no.)	Main Data
Deeper GNSS CHIRP+	SPP	28,800	28,800	Latitude, longitude
Deeper GNSS Pro+ 2	SPP	28,800	28,800	Latitude, longitude
G > S > P Sys	SPP	28,800	28,800	Latitude, longitude, ellipsoid height
	Post-Processing Static	28,800	28,800	Latitude, longitude, ellipsoid height
	PPP	28,800	28,800	Latitude, longitude, ellipsoid height

2.3.2. Dynamic Datasets

To construct the datasets for the evaluation of Deeper Smart Sonar Pro+ 2 and CHIRP+ and the G > S > P Sys in kinematic positioning, a sea test and a test in an open pool were performed.

The sea test was performed on the coast of Mar Grande, Taranto, Italy (Lat.: 40°25'23.32" N; Long.: 17°12'53.01" E). The place is rich in beaches, has shallow water for many metres and is protected by breakwaters. The purpose of the test was to compare the planimetric positioning performance of the Deeper Smart Sonars and the G > S > P Sys. The test consisted of moving the devices along a straight path of approximately 11.50 metres from point A to point B. The points were identified by inserting stakes and to facilitate the operator, additional intermediate stakes were inserted to form a corridor. For comparison, the path was surveyed using traditional methods and a GNSS survey.

The pool test (Figure 2a) was conducted to study in detail the performance of the G > S > P Sys considered to be more precise and accurate than the Deeper Smart Sonars after the first tests. In the test, the G > S > P Sys surveyed the four sides of a rectangular swimming pool (largest side = 8.95 m, smallest side = 4.47 m, surface area~40.01 sqm) using the edges of the structure as a guide. For comparison, the pool was surveyed using traditional methods (rigid metric ruler, metric roll, laser distance meter, etc.) and a static GNSS survey.

To conduct the tests, the instrumentation was mounted on a small floating platform (prototype zero) built for experimental purposes (Figure 2b). The platform allowed flotation via the high-density foam base, waterproofing and control of the instrumentation via the transparent container, the possibility of mounting both the G > S > P Sys antenna and the smartphone on the stand, and continuous contact between the Deeper Smart Sonars and water using a part of “flexible arm mount 2.0” by Deeper UAB.

The sea test produced five datasets: (i) Deeper Smart Sonar CHIRP+ with the planimetric positioning data in real-time in SPP, (ii) Deeper Smart Sonar Pro+ 2 with the planimetric positioning data in real-time in SPP, (iii) G > S > P Sys with the planimetric positioning data

in real-time in SPP, (iv) G > S > P Sys with the planimetric positioning data in PPP-kinematic, (v) G > S > P Sys with the planimetric positioning data in PPK.

The pool test produced three datasets containing the 3D positioning data for the G > S > P Sys in real-time in SPP, in PPP-kinematic and in PPK.

Table 4 shows the composition of the dynamic datasets built in the sea test and Table 5 shows the composition of the dynamic datasets built in the pool test.

Table 4. Dynamic datasets composition of the sea test.

Path Length [m]	Device	Positioning	Data Sample (no.)	Main Data
~11.50 linear	Deeper GNSS CHIRP+	SPP	150	Latitude, longitude
	Deeper GNSS Pro+ 2	SPP	150	Latitude, longitude
	G > S > P Sys	SPP	150	Latitude, longitude
		PPP-kinematic	150	Latitude, longitude
		PPK	150	Latitude, longitude

Table 5. Dynamic datasets composition of the pool test.

Path Length [m]	Device	Positioning	Data Sample (no.)	Main Data
~26.84 rectangular	G > S > P Sys	SPP	1000	Latitude, longitude, ellipsoidal height
		PPP-kinematic	1000	Latitude, longitude, ellipsoidal height
		PPK	1000	Latitude, longitude, ellipsoidal height



(a)



(b)

Figure 2. (a) Pool test; (b) instrumentation mounted on the floating platform.

2.3.3. Water Depth Datasets

Two different tests were performed to evaluate the accuracy and precision of the Deeper Smart Sonar CHIRP+ and Pro+ 2 in measuring water depth.

The first test was conducted in a swimming pool to evaluate the performance of the sonar in fresh water and under controlled conditions (purified and transparent water, obstacle-free bottom and no waves). The second test was conducted in the sea to evaluate depth measurements in salt water and under operating conditions (the sites were the same as those indicated in Section 2.3.2.). During the two tests, the depths of two points were measured with sonar, one at 0.9 m and one at 1.52 m corresponding to the minimum and maximum depths of the pool. For the comparison between sonar measures and ground-truths, the points in the pool and in the sea were also measured using classical methods,

such as a rigid metre, a graduated pole and a weighted metric roll [7,8]. The tests were performed with a water temperature as constant as possible between them. The mean salinity of the Mar Grande in Taranto, the test site, can be considered to be ~37.8‰ [37,38]. In the tests, the “flexible arm mount 2.0” by Deeper UAB was used to ensure constant immersion of the sonar in the water. This accessory allows the sonar to be fixed to boats, kayaks and, as in this case, to the edge of the pool and Stand Up Paddle board (SUP).

Table 6 shows the composition of the water depth datasets.

Table 6. Water depth datasets composition.

Device	Real Depth (m)	Water	Temperature (°C)	Data Sample (no.)	Main Data
Deeper Smart Sonar CHIRP+	0.9	Fresh Salt~37.8‰	22.27 20.90	3700 3700	Depth Depth
	1.52	Fresh Salt~37.8‰	22.27 20.90	3700 3700	Depth Depth
Deeper Smart Sonar Pro+ 2	0.9	Fresh Salt~37.8‰	22.27 20.90	3700 3700	Depth Depth
	1.52	Fresh Salt~37.8‰	22.27 20.90	3700 3700	Depth Depth

2.3.4. Building of the Datasets for 3D Modelling

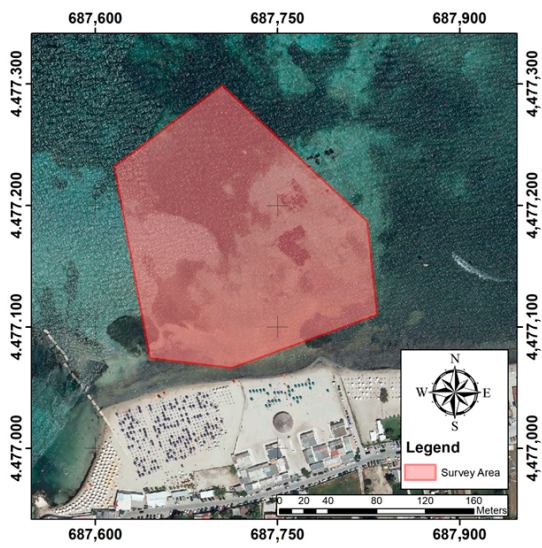
The surveys performed for the construction of the datasets for 3D modelling were conducted with the Deeper Smart Sonar CHIRP+ implemented in the G > S > P Sys (as in Figure 1).

The dataset for 3D modelling of artificial structures, in this case, a swimming pool with bottom variation, was constructed by surveying the pool used in the tests in Section 2.3.2. The dataset for the 3D modelling of the natural surfaces was constructed by a seabed survey in the site indicated in Section 2.3.2. The survey covered an area of about 3 hectares (about 2 beaches) with the most distant point from the coast surveyed at about 240 m (Figure 3a). For the survey, 16 transects orthogonal and 1 parallel transect to the coast were executed, and 1659 points were collected. The survey was conducted semi-automatically by “creating” the map in real-time by executing transects according to the areas of the map to be completed indicated by the Fish deeper—Fishing App. This survey mode can be compatible with cost-efficient science projects and citizen science projects, for example.

The survey was conducted using a SUP board (Figure 3d–f) with a new floating platform connected to it (prototype 3—Figure 3b,c). The new low-cost platform had a trimaran structure for greater stability in navigation, and an “F” bracket was installed at the stern to planimetrically align the external GNSS antenna with the Sonar (Figure 3b–d—in green circle).

In order to facilitate the exposition in Section 2.4, dedicated to 3D modelling, the file downloaded from the Deeper Smart Sonar CHIRP+ was called “File Sonar”, the file containing the real-time positioning data in SPP of the SimpleRTK2B was called “File SPP” and the file containing the post-processed positioning data in PPK of the SimpleRTK2B was called “File PPK”.

Table 7 shows the composition of the datasets for 3D modelling of the seabed (natural surface) and Table 8 shows the composition of the datasets for 3D modelling of the pool (artificial structure).



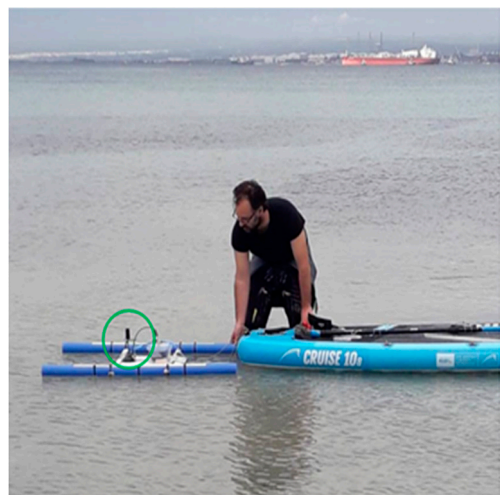
(a)



(b)



(c)



(d)



(e)



(f)

Figure 3. (a) Survey area at sea; (b) preparation of instruments; (c) floating platform; (d) preparation of SUP for the survey; (e) floating platform connected to SUP; (f) survey at sea.

Table 7. Datasets for 3D modelling of the seabed (natural surface).

Area Surveyed (sqm)	Transects (no.)	Device	File Produced	Positioning	Points Surveyed (no.)	Main Data
~30,000	16 + 1	Deeper GNSS CHIRP+	File Sonar	SPP	1659	Latitude, longitude, depth
		SimpleRTK2B	File SPP	SPP	6098	Latitude, longitude, ellipsoidal height, GPST
			File PPL	PPK	6098	Latitude, longitude, ellipsoidal height, GPST

Table 8. Datasets for 3D modelling of the pool (artificial structure).

Area Surveyed (sqm)	Transects (no.)	Device	File Produced	Positioning	Points Surveyed (no.)	Main Data
~40.01	2 + 2	Deeper GNSS CHIRP+	File Sonar	SPP	111	Latitude, longitude, depth
		SimpleRTK2B	File SPP	SPP	982	Latitude, longitude, ellipsoidal height, GPST
			File PPL	PPK	982	Latitude, longitude, ellipsoidal height, GPST

2.4. 3D Data Modelling

This section describes in detail the implementation of the pipeline for the creation of the 3D models of the datasets produced in Section 2.3.4. The seabed was modelled as representing the natural surfaces and a pool with a variable bottom as representing the artificial structures. As mentioned in Section 2.1, the modelling consisted of three steps: synchronisation, interpolation and 3D modelling. Figure 4 shows the synthetic pipeline for 3D modelling with the main software used for implementation.

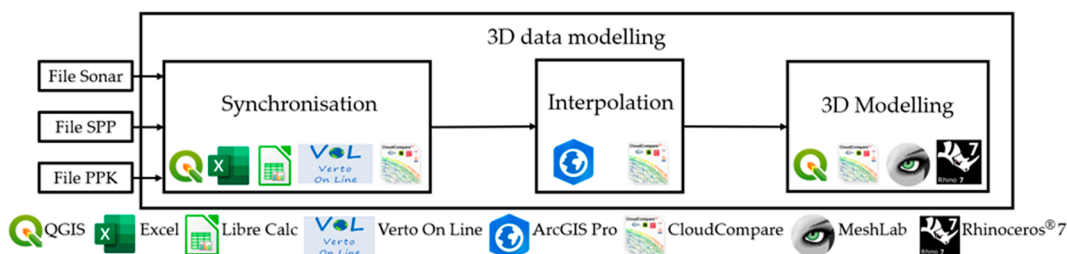


Figure 4. Implementation of the pipeline for 3D modelling of bathymetric data derived from the G > S > P Sys.

2.4.1. Synchronisation

The synchronisation was performed in the open-source software QGIS (QGIS Development Team) using the geoprocessing algorithm of joining attributes between fields (ID algorithm: ‘native:joinattributable’). Some secondary data processing was performed using spreadsheets in software such as Excel (Microsoft, Redmond, Washington, USA) and Libre Calc (The Document Foundation).

The synchronisation followed:

1. The File Sonar was synchronised with the File SPP via the latitude and longitude fields, the new file was named “File Sonar + SPP” (through this synchronisation, the File Sonar was associated with the GPS Time value of the system);
2. The File Sonar + SPP was synchronised with the File PPK via the common GPS Time field. Figure 5a shows a detail of the pre-synchronisation File Sonar + SPP in orange and the File PPK in red. The new file produced was called “File Sonar + SPP + PPK” and contained the information on latitude, longitude and ellipsoid height corrected

to PPK, depth of water and time of point acquisition. Figure 5b shows a comparison between the File Sonar + SPP + PPK in green and the File PPK in red.

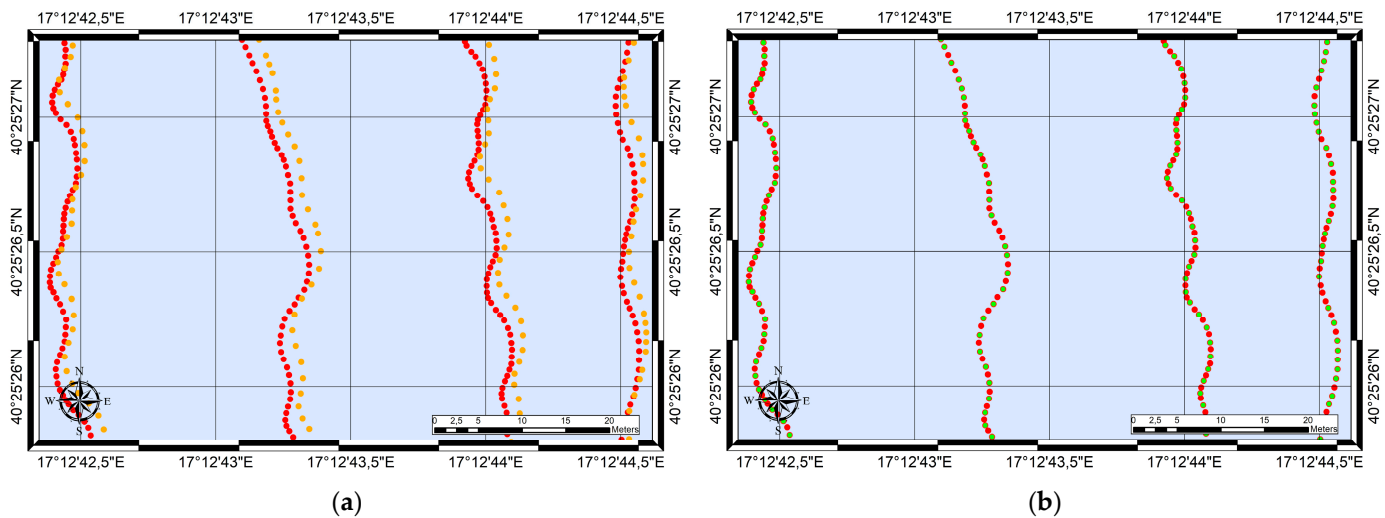


Figure 5. (a) Comparison between File Sonar + SPP (in orange) and File PPK (in red); (b) comparison between Sonar + SPP + PPK (in green) and File PPK (in red).

Generally, after the synchronization, the File Sonar + SPP + PPK may be processed as follows:

1. Correction of the offset between the GNSS antenna and sonar transducer;
2. Correction of the offset between the sonar transducer and keel line;
3. Selection of the vertical reference system, for example, tidal observations (Mean Sea Level—MSL, Lowest Astronomical Tide—LAT, etc.), physical model (geoid) or reference ellipsoid [17];
4. Correction of the water level variations.

In this specific case study, the planimetric offset between the GNSS antenna and sonar transducer was originally annulled by the floating platform. Concerning the vertical reference, it was decided to use a physical reference on land, that is the tide gauge of Taranto, part of the National Mareographic Network and located in the Mar Grande a few kilometres from the surveyed site. The water level variations corrections were deduced from the tide gauge data. In order to be able to subsequently process the dataset in CloudCompare (DF R&D/TELECOM ParisTech ENST-TSI, Paris, France) [39], the GNSS coordinates of the surveyed points were converted into the WGS 84/UTM 33N system with the VERTO software (Istituto Geografico Militare—IGM, Florence, Italy).

Finally, a random sample of 1000 points (approximately 60% of the surveyed points) was extracted for 3D modelling; the remaining 40% of the points were used in the model validation phase.

2.4.2. Interpolation

As mentioned in Section 2.1, the main interpolation was performed with the ArcGIS Pro software and the Forest-based Classification and Regression method was used.

The processes performed for the interpolation of data via Forest-based Classification and Regression were:

1. Parameter definition and creation of a first bathymetric grid interpolated using the IDW method (Figure 6c);
2. Definition of the training features for the Forest-based Classification and Regression method;
3. Training, algorithm running and producing the final bathymetric grid interpolated by Forest-based Classification and Regression method (grid FCR).

In the second process, the input training features were the bathymetric points surveyed (Input Training Features), the variable to predict was the depth (Variable to Predict) and the explanatory training variable was the bathymetric grid IDW (Explanatory Training Rasters).

Figure 6a shows the grid FCR produced by the Forest-based Classification and Regression method (1×1 m cell). Figure 6b,c show the additional grids used for comparison in the analysis phase. Specifically, Figure 6b shows the bathymetric grid obtained by applying the Ordinary Kriging interpolation method (grid OK) and Figure 6c the bathymetric grid obtained with the IDW interpolation method (grid IDW). The values shown in Figure 6 correspond to the value of depth (in meters) in relation to the water level.

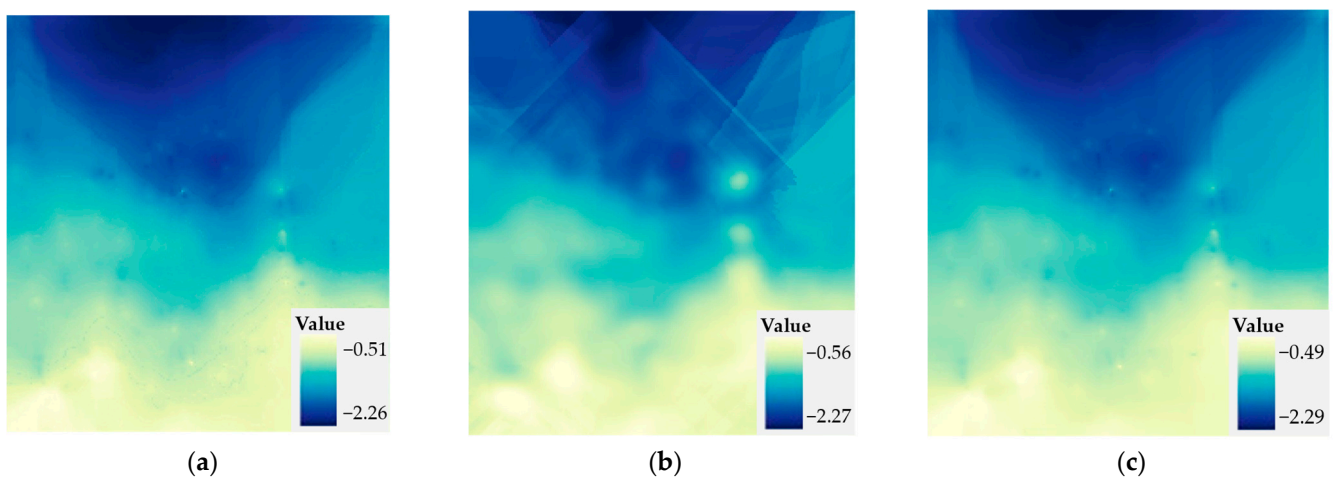


Figure 6. Bathymetric grid models produced by interpolation: (a) grid produced by Forest-based Classification and Regression method (grid FCR); (b) grid produced by Ordinary Kriging method (grid OK); (c) grid produced by IDW method (grid IDW).

2.4.3. 3D Modelling of Natural Surface

The 3D mesh modelling was performed using the software: QGIS 3.22.8, CloudCompare and Meshlab (Visual Computing Lab-ISTI-CNR, Pisa, Italy) [40]. The bathymetric grids of Section 2.4.2. (grid FCR, grid OK and grid IDW) were imported into QGIS and transformed into punctual shapefiles. Each point was associated with the depth value of the cell and the coordinates in the WGS84/UTM 33N system (ID algorithms: 'native:pixelstpoints' and 'native:addxyfields'). Subsequently, the layers were exported in text format (*.csv). During this step, it was possible to add additional information to the files in order to generate 3D models with depth exaltation, a type of representation used to visualise large surfaces (or lengths) with small variations in height (some modelling examples are shown in Figure 7). Then the files were converted into Polygon File Format (*.ply, a specific format for 3D object representation) via CloudCompare, generating the point clouds (Figure 7a–c). After, the files were imported into Meshlab for 3D modelling. In Meshlab, point cloud normals were generated and then the point clouds were modelled into 3D models tri-mesh using the Poisson surface reconstruction method (Figure 7d–f). Finally, the textures of the bathymetric grids of Section 2.4.2. were applied in Meshlab to improve the readability of the models (Figure 7g–i). In order to facilitate exposition, the 3D model created using the grid FCR was called 3D model FCR, the 3D model created using the grid OK was called 3D model OK and the 3D model created using the grid IDW was called 3D model IDW.

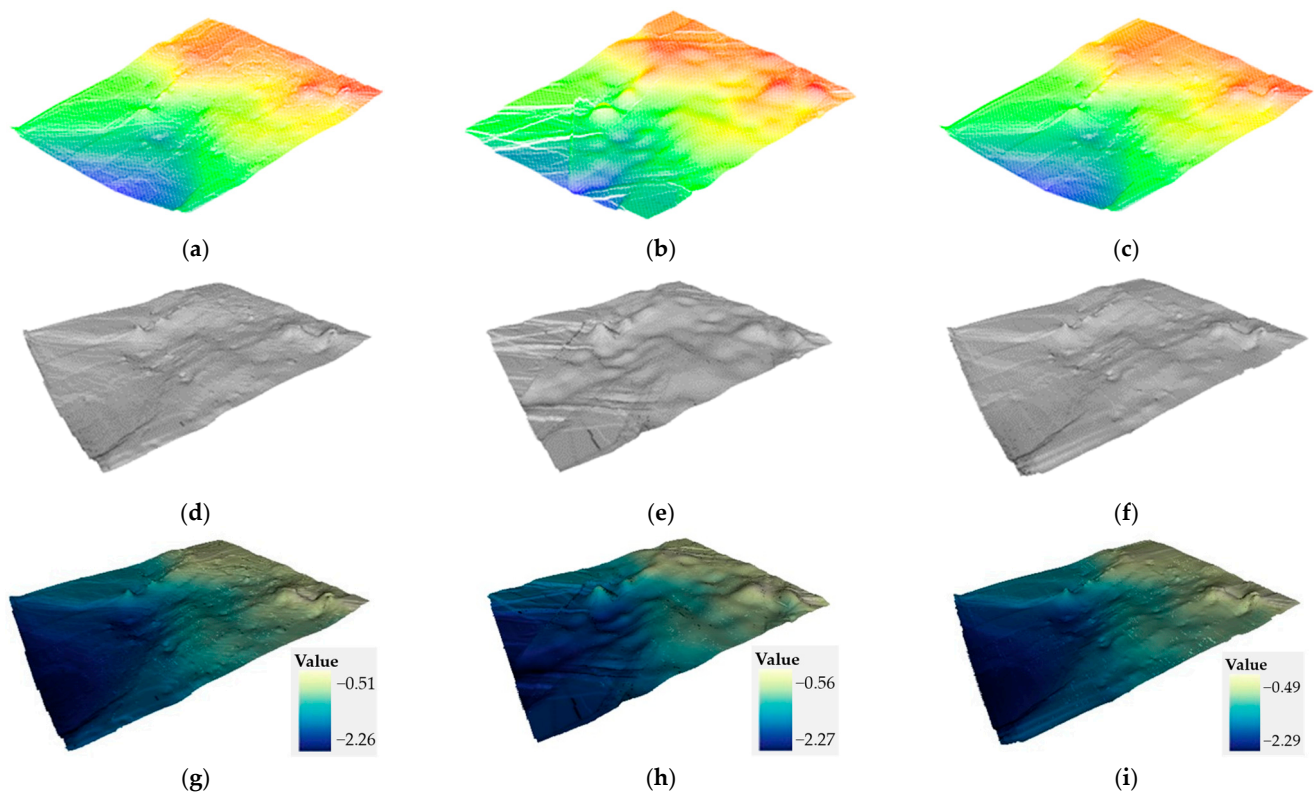


Figure 7. Modelling examples: (a) point cloud FCR; (b) point cloud OK; (c) point cloud IDW; (d) 3D model FCR; (e) 3D model OK; (f) 3D model IDW; (g) textured 3D model FCR; (h) textured 3D model OK; (i) textured 3D model IDW.

2.4.4. 3D Modelling of Artificial Structure

Concerning the 3D modelling of artificial structures, the software used was CloudCompare and Rhinoceros[®] 7 (Robert McNeel & Associates, Seattle, Washington, USA). In the 3D modelling of the swimming pool, the GNSS data and sonar data were synchronised in accordance with the step described in Section 2.4.1. However, since the survey was conducted with the first prototype floating platform, an offset correction between the GNSS antenna and Sonar was performed and the overflow side of the full pool was assumed as a vertical reference. In the interpolation phase, as the area to be reconstructed was small, the bottom point cloud was generated by linear interpolation of the nearest non-empty neighbouring cells.

Figure 8a shows the point cloud obtained after the synchronisation and correction operations, the emerged edges derive from the GNSS data while the bottom derives from the G > S > P Sys data. The missing parts (in red circles) refer to the pool ladders that were not surveyed. Figure 8b shows the bottom of the pool reconstructed by interpolation; this operation was necessary to give longitudinal continuity to the sonar data for subsequent slicing operations. Figure 8c shows the 3D model of the pool surveyed with traditional techniques and assumed as the ground-truth in the analysis phase.

Since the structure to be modelled had a well-defined shape, data-driven modelling by a primitives approach was used.

In CloudCompare by Cross Section tool, the contour lines for the creation of the primitives were generated by extracting the sections of the pool edge and the bottom. In order to regularise the contour line of the pool edge, the contour line regularisation via mesh plane, previously described [18], was performed (Figure 9).

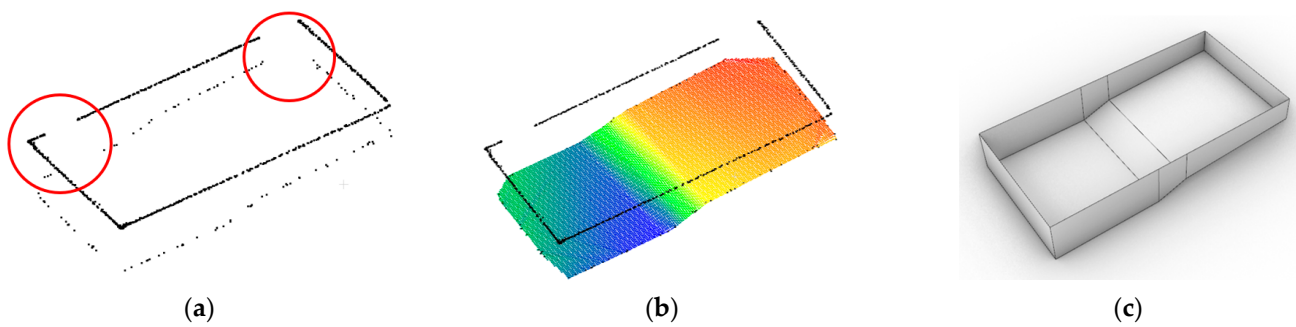


Figure 8. (a) Point cloud after synchronisation and correction operations; (b) interpolated pool bottom; (c) 3D model of the pool surveyed using traditional methods.

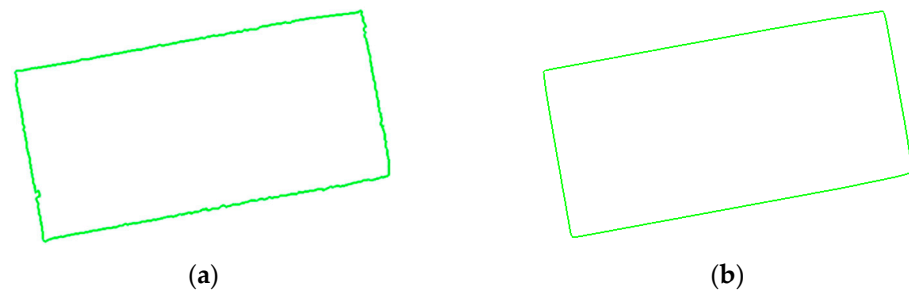


Figure 9. (a) Pool edge contour line before regularization; (b) pool edge contour line after regularization.

The contour lines were imported into Rhinoceros[®] v.7 software for the creation of the primitives and the final 3D modelling. The primitives representing the pool walls and bottom were automatically generated by the commands: ExtrudeCrv and ExtendSrf (Figure 10a). Finally, based on the primitives, the 3D model was created by the commands: Intersect, Meshpolyline and Loft (Figure 10b).

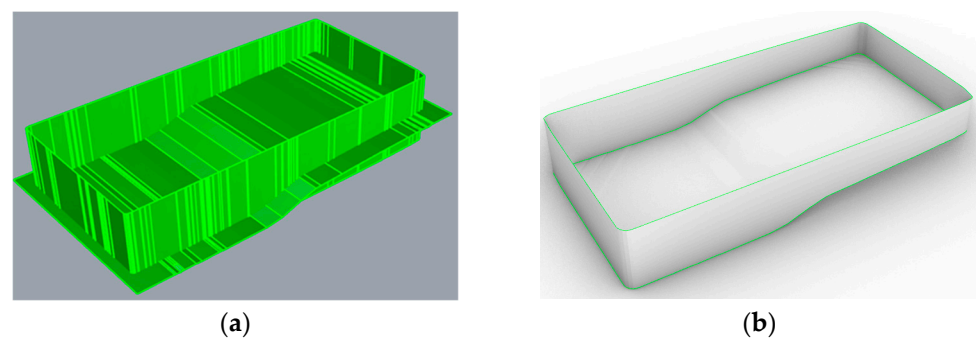


Figure 10. (a) Primitives representing the walls and bottom of the pool; (b) final 3D model of the pool.

3. Results

This section reports the results obtained during the tests performed to evaluate the static and kinematic GNSS positioning, the accuracy and precision of depth measurements, and the quality of the 3D models produced. In the exposure, the values of Total Horizontal Uncertainty (THU) at a 95% of confidence level and Total Vertical Uncertainty (TVU) at a 95% of confidence level were calculated according to the sixth edition of IHO Standards for Hydrographic Surveys [17] by formulas:

$$TVU = 1.96 \cdot \sigma V \quad (7)$$

$$THU = 2.45 \cdot \sigma 2D \quad (8)$$

where σ_V is the vertical Standard Deviation, e.g., in the case of the depth measurement, and σ_{2D} is the horizontal Standard Deviation, e.g., in the case of the planimetric GNSS positioning. In cases where the positioning values were reported in the two coordinates North and East (σ_N for the North and σ_E for the East), the worst σ value of the two was used, since the standard assumes the THU expressed by a single value.

3.1. GNSS Positioning Test Results

This section reports data collected under static and kinematic conditions to evaluate the geolocation performance of the GNSS receivers studied. Table 9 shows the real-time static Single Point Positioning (SPP) values of the GNSS receivers of the Deeper Smart Sonar CHIRP+ (Deeper GNSS CHIRP+), Deeper Smart Sonar Pro+ 2 (Deeper GNSS Pro+ 2) and G > S > P Sys (G > S > P Sys). The observation time for the three devices was 8 h (28,800 s). The value of Δ , in the components North (ΔN), East (ΔE) and Up (ΔU), represents the mean distance between the surveyed point P and FATA (known coordinates). σ is the standard deviation of the GNSS positioning of the receivers in P in the components North (σ_N), East (σ_E) and Up (σ_U).

Table 9. Performance in real-time static SPP of Deeper Smart Sonar CHIRP+, Deeper Smart Sonar Pro+ 2 and G > S > P Sys.

Device	Positioning	Obs. Time (s)	ΔN (m)	ΔE (m)	ΔU (m)	σ_N (m)	σ_E (m)	σ_U (m)	THU (m)
Deeper GNSS CHIRP+	SPP	28,800	2.621	0.761	ND	0.877	0.624	ND	2.150
Deeper GNSS Pro+ 2	SPP	28,800	3.537	1.706	ND	0.674	0.980	ND	2.401
G > S > P Sys	SPP	28,800	2.484	0.570	2.018	0.194	0.199	0.659	0.487

For easier graphical evaluation, Figure 11 shows the real-time static planimetric SPP accuracy ($\Delta 2D$) of the G > S > P Sys during an observation time of 1 h (3600 s).

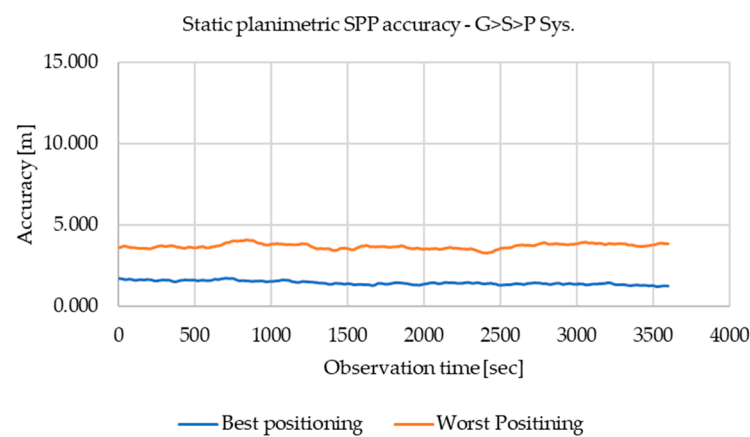


Figure 11. Accuracy (best and worst) in real-time static planimetric SPP of the G > S > P Sys during 3600 s.

In blue is reported the best positioning recorded during the 8 h of observation and in orange the worst positioning. The accuracy was calculated using the formula:

$$\Delta 2D = \sqrt{\Delta E^2 + \Delta N^2} \tag{9}$$

For comparison, Figures A1 and A2 in Appendix A show the real-time static SPP planimetric positioning accuracy of the Deeper Smart Sonar CHIRP+ and the Deeper Smart Sonar Pro+ 2. Figure 12 shows the Signal-to-Noise Ratio (SNR) of the G > S > P Sys. A high SNR corresponds to better measurement. The images show the SNR for L1 and L2 for best and worst positioning expressed in Figure 11 (for 3600 s). Figure A3 (in Appendix A), shows the SNR values for the Huawei P30 Pro (for L1 and L5) for comparison.

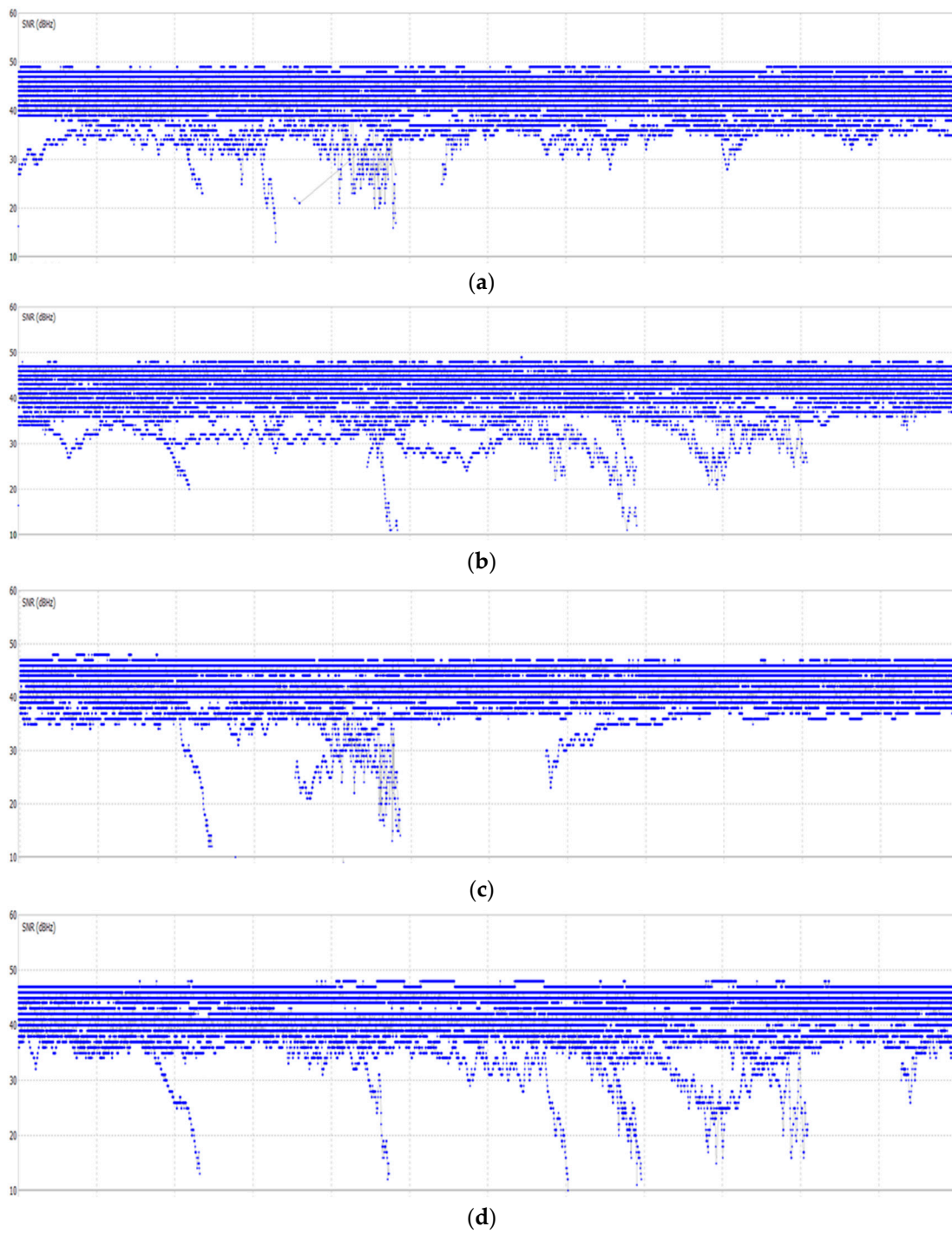


Figure 12. For the $G > S > P$ Sys: (a) Best SNR for L1; (b) worst SNR for L1; (c) best SNR for L2; (d) worst SNR for L2.

Table 10 shows the GNSS static positioning data, post-processed in static and PPP mode of the $G > S > P$ Sys. The values of Δ and σ are based on observations of 5 min (300 s), 15 min (900 s), 30 min (1800 s) and 1 h (3600 s) of eight samples collected during 8 h of observation.

Table 10. Performance in static positioning post-processed in static mode and PPP mode of the G > S > P Sys.

Device	Positioning	Obs. Time (s)	ΔN (m)	ΔE (m)	ΔU (m)	σN (m)	σE (m)	σU (m)	THU (m)
G > S > P Sys	Post-Processing Static	300	0.001	0.006	0.031	0.002	0.002	0.004	0.005
		900	0.001	0.006	0.030	0.002	0.002	0.005	0.005
		1800	0.001	0.006	0.031	0.001	0.002	0.006	0.004
		3600	0.001	0.006	0.031	0.001	0.001	0.006	0.003
	PPP	300	0.667	0.632	0.249	0.474	0.906	1.107	2.220
		900	0.639	0.712	0.074	0.134	0.317	0.320	0.778
		1800	0.636	0.765	0.043	0.058	0.143	0.148	0.352
		3600	0.646	0.750	0.026	0.010	0.022	0.033	0.053

For easier interpretation, Figure 13 shows a synthetic diagram representing the evolution of the accuracy in static planimetric post-processing positioning of the G > S > P Sys during 3600 s. In grey are represented the data post-processed in static mode and in yellow the data post-processed in PPP mode. For completeness, Figure A4 (in Appendix A) shows the diagram of 3D positioning accuracy.

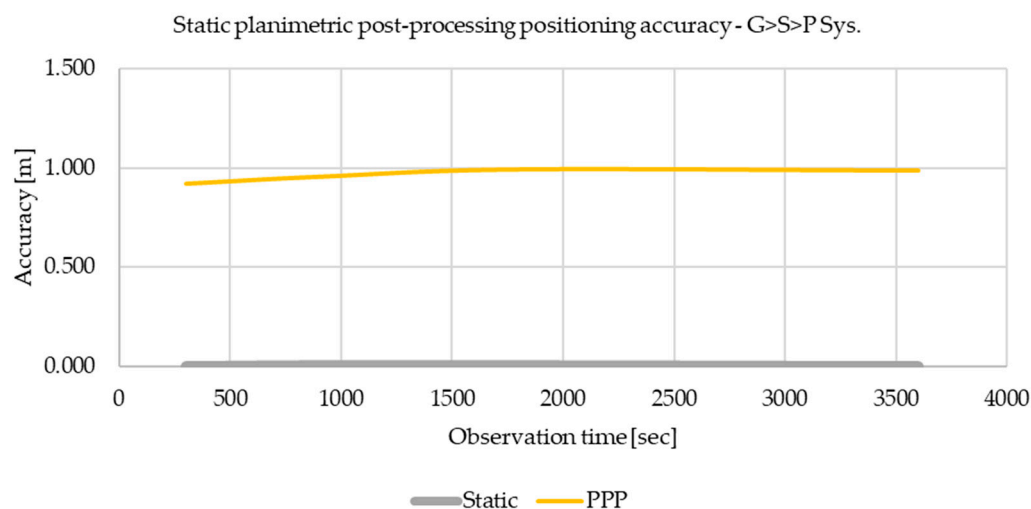


Figure 13. Accuracy in static planimetric post-processing positioning in static mode (grey) and in PPP mode (yellow) of the G > S > P Sys.

Tables 11 and 12 show the data regarding the GNSS kinematic positioning tests of the Deeper Smart Sonar CHIRP+, the Deeper Smart Sonar Pro+ 2 and the G > S > P Sys. In particular Table 11 shows the data from the test performed in the sea and Table 12 shows the data from the test performed in the pool. Based on the tests performed, for the Deeper Smart Sonars (CHIRP+ and Pro+ 2) the SPP data of the sea test are reported.

For the G > S > P Sys the SPP, PPP-kinematic and PPK data for the sea and pool tests are reported. The $\mu 2D$ and $\mu 3D$ values report the mean distance of the set of surveyed points in relation to the trajectory travelled in planimetric and 3D, $\sigma 2D$ and $\sigma 3D$ are the respective standard deviations in planimetric and 3D.

In order to evaluate the dispersion of the points surveyed in the pool test, Figure 14 shows a comparison between the G > S > P Sys positioning data and the real trajectory travelled. In these figures the real trajectory is shown in green; in particular, Figure 14a,d show the SPP data in planimetric and 3D, respectively, Figure 14b,e show the PPP-kinematic positioning data in planimetric and 3D, respectively and Figure 14c,f show the PPK positioning data in planimetric and 3D, respectively.

Figure A5, in Appendix A, shows the dispersion of the points surveyed in the sea test.

Table 11. Performance in the GNSS kinematic planimetric positioning of the Deeper Smart Sonar CHIRP+, the Deeper Smart Sonar Pro+ 2 and the G > S > P Sys in the sea test.

Path Length (m)	Device	Positioning	μ 2D (m)	σ 2D (m)	THU (m)
~11.50 linear	Deeper GNSS CHIRP+	SPP	2.007	1.911	4.682
	Deeper GNSS Pro+ 2	SPP	0.700	0.482	1.180
	G > S > P Sys	SPP	1.034	0.095	0.232
		PPP-kinematic	0.640	0.092	0.226
		PPK	0.043	0.031	0.075

Table 12. Performance in the GNSS kinematic positioning of the G > S > P Sys in the pool test.

Path Length (m)	Device	Positioning	μ 2D (m)	σ 2D (m)	μ 3D (m)	σ 3D (m)	THU (m)
~26.84 rectangular	G > S > P Sys	SPP	0.438	0.390	0.524	0.350	0.956
		PPP-kinematic	0.417	0.309	0.465	0.290	0.757
		PPK	0.037	0.040	0.061	0.060	0.098

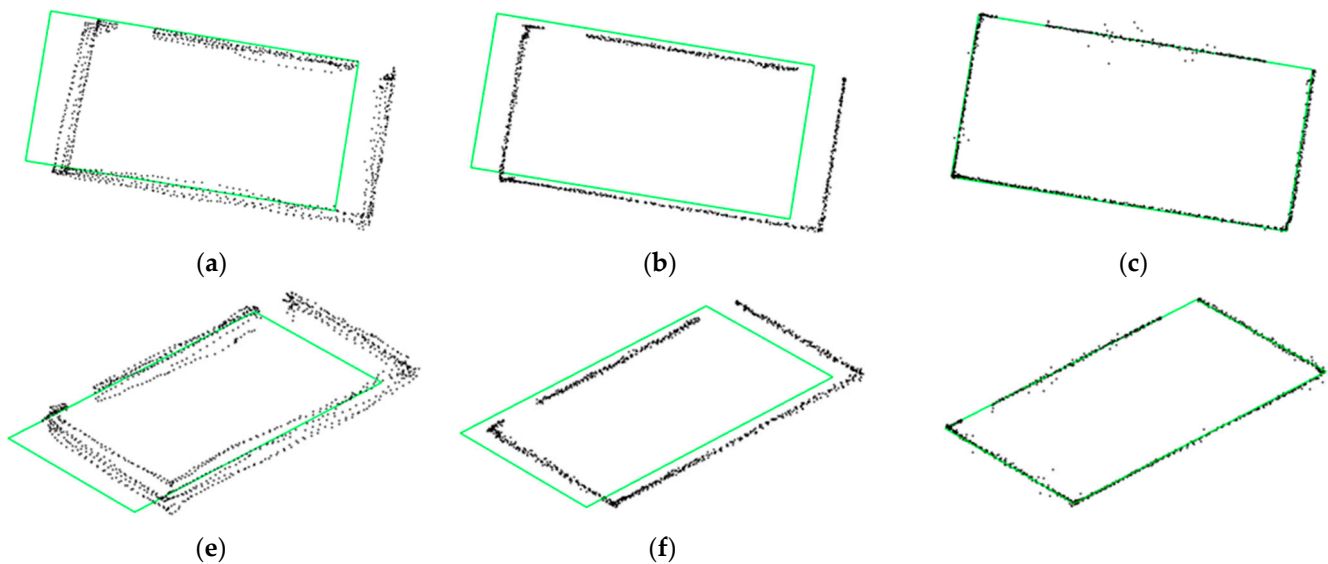


Figure 14. Comparison of the GNSS kinematic positioning of the G > S > P Sys in the pool test: (a) planimetric SPP; (b) planimetric PPP-kinematic positioning; (c) planimetric PPK positioning; (d) 3D P; (e) 3D PPP-kinematic positioning, (f) 3D PPK positioning.

3.2. Depth Survey and 3D Modelling Test Results

This section reports the data to evaluate the sonar performance in depth measurement and the 3D modelling methods.

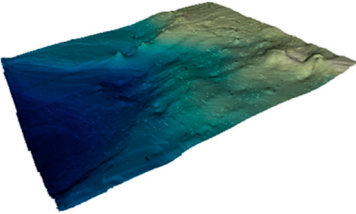
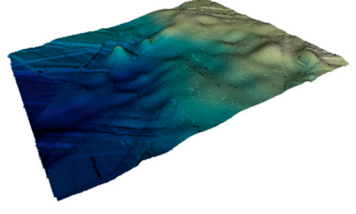
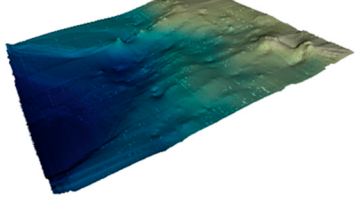
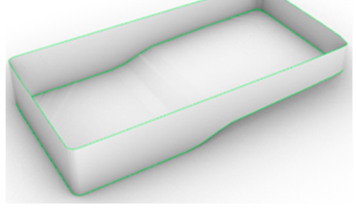
Table 13 shows the data collected to evaluate the performance of the Deeper Smart Sonars CHIRP+ and Pro+ 2 in measuring depth. The measured depths were 0.9 m and 1.52 m, in fresh and sea water (salinity 37.8‰). The value of ΔV represents the difference between the mean of the measured depth value considering 3700 samples and the real depth value, σV is the standard deviation of the measured values.

To evaluate the accuracy and precision of the 3D models produced, a comparison based on Cloud-To-Mesh (C2M) distance was performed in CloudCompare (Table 14).

Table 13. Performance in depth measurement of Deeper Smart Sonar CHIRP+ and Deeper Smart Sonar Pro+ 2.

Device	Real depth (m)	Water	ΔV (m)	σV (m)	TVU (m)
Deeper Smart Sonar CHIRP+	0.9	Fresh Salt~37.8‰	0.02 0.02	0.00 0.02	0.00 0.04
	1.52	Fresh Salt~37.8‰	0.01 0.01	0.00 0.11	0.00 0.21
Deeper Smart Sonar Pro+ 2	0.9	Fresh Salt~37.8‰	0.03 0.02	0.00 0.02	0.00 0.04
	1.52	Fresh Salt~37.8‰	0.02 0.04	0.00 0.06	0.01 0.12

Table 14. Mean and standard deviation values of C2M distance of seabed and pool models.

Model	Example Images	Interpolation Method	$\mu 3D$ (m)	$\sigma 3D$ (m)
3D model FCR – natural surface		Forest-based Classification and Regression	0.0020	0.0323
3D model OK – natural surface		Ordinary Kriging	0.0043	0.0283
3D model IDW – natural surface		IDW	0.0059	0.0317
3D model pool – artificial structure		Linear interpolation	0.0124	0.0245
3D model bottom pool – artificial structure		Linear interpolation	0.0002	0.0140

For the seabed (the natural surfaces), the comparison was carried out between the 3D model FCR, the 3D model OK and the 3D model IDW, and 40% of the points that were selected for the final validation. In the case study of the pool (the artificial structure), a comparison was conducted between the 3D model created by the proposed 3D modelling method and the model reconstructed by the traditional survey. Furthermore, regarding the swimming pool, the C2M was performed both on the entire structure and only on the bottom.

In Table 14, μ_{3D} is the mean distance C2M, and σ_{3D} is the corresponding standard deviation.

In order to make some observations on the interpolation and 3D modelling methods used, Figure 15 shows three illustrative vertical sections executed on the three 3D models of the seabed. The points used for validation were represented as black squares, the section of the 3D model FCR was represented in blue, the section of the 3D model OK was represented in orange and the section of the 3D model IDW was represented in red. Figure 15a shows the three sections and Figure 15b,c show the disaggregated data to facilitate comparison between the models (3D model FCR vs. 3D model IDW in Figure 15b and 3D model FCR vs. 3D model OK in Figure 15c).

Finally, Figure A6 (in Appendix A) shows the histograms of the analysis performed on the pool.

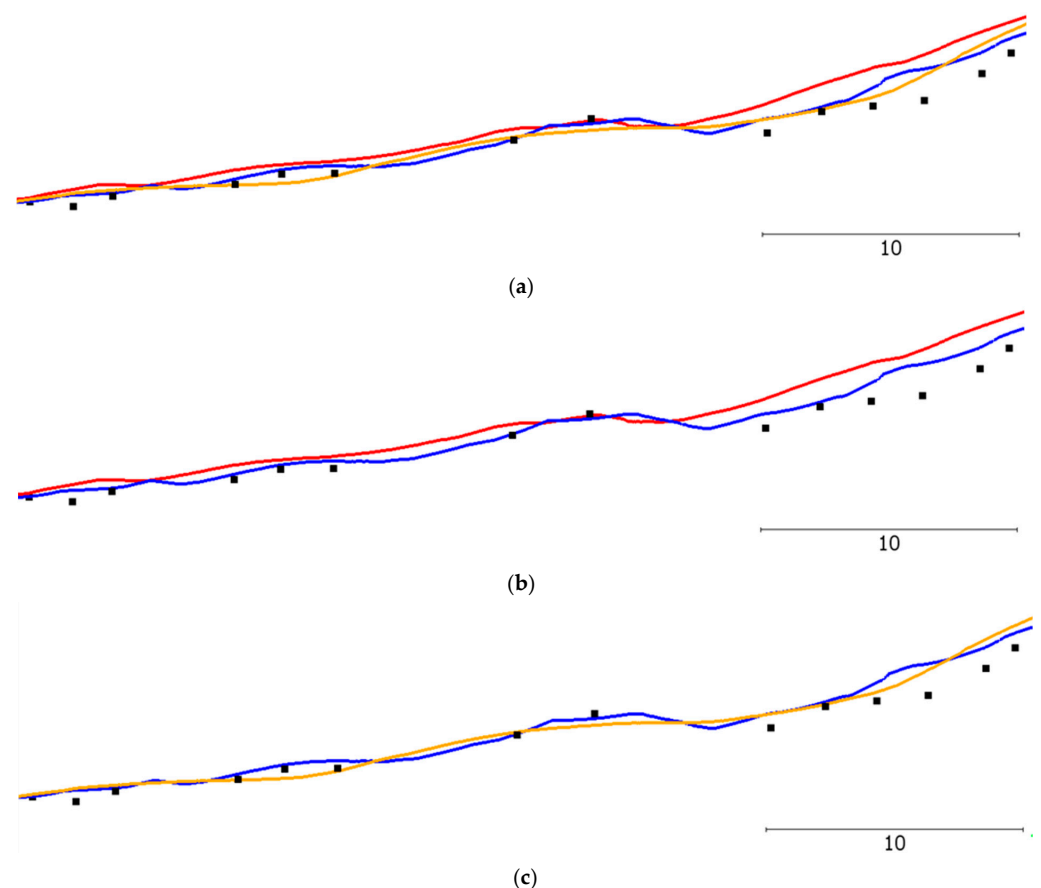


Figure 15. Comparative longitudinal vertical sections executed on the 3D models, the black squares represent the points used for validation: (a) comparison between the 3D model FCR (in blue), the 3D model OK (in orange) and the 3D model IDW (in red); (b) comparison between the 3D model FCR (in blue) and the 3D model IDW (in red); (c) comparison between the 3D model FCR (in blue) and the 3D model OK (in orange).

4. Discussion

Comparing the best and worst TVU values (0.00 and 0.21 m) reported in Table 13 with the TVU IHO standards [17] (see Table 15), it can be seen that the Deeper Smart Sonars produced depth measurements with a TVU between the Exclusive Order and the Special Order.

Regarding the geolocation of the devices in the static tests, it can be observed that in the SPP (Table 9 and Figures 11, A1 and A2) the G > S > P Sys was superior in comparison to the Deeper Smart Sonars. In the post-processing (Table 10, Figures 13 and A4) the static was superior compared to the PPP static.

In the dynamic tests, analysing the THU values of the Deeper Smart Sonars, as shown in Table 11 (1.180 and 4.682 m), and comparing them with the reference THU standards values in Table 15 [17], it can be observed that the Deeper Smart Sonars obtained values between the Special Order and the Order 1. Observing the values of the G > S > P Sys shown in Tables 11 and 12 and Figure 14, it can be seen that in all types of positioning performed (SPP, PPP kinematic and PPK), the THU values are compatible with the Exclusive Order (the worst value is in fact 0.956 m). The dispersion of the surveyed points (Figure A5) in SPP had a minor dispersion compared to the Deeper Smart Sonars. In addition, an analysis of Figures 12 and A3 reveals that the SNR of the G > S > P Sys is in each case better than the internal GNSS receiver of the Huawei P30 Pro.

Considering overall the THU and TVU values of the Deeper Smart Sonars it can be deduced that these sensors can express uncertainty values that in the worst case are compatible with the Order 1 and in the best case with the Special Order. Instead, the G > S > P Sys in the worst case can express uncertainty values compatible with the Special Order and in the best case with the Exclusive Order.

Table 15. THU e TVU bathymetry IHO standards for safety of navigation hydrographic surveys [17].

Criteria	Order 2	Order 1 (a/b)	Special Order	Exclusive Order
THU	20 m + 10% of depth	5 m + 5% of depth	2 m	1 m
$\sqrt{a^2 + (b \cdot d)^2}$	a = 1.0 m b = 0.023	a = 0.5 m b = 0.013	a = 0.25 m b = 0.0075	a = 0.15 m b = 0.0075

In TVU, *a* is the portion of the uncertainty that does not vary with depth, *b* is a coefficient representing the portion of uncertainty that varies with depth and *d* is the depth.

The μ 2D values of the Deeper Smart Sonar internal GNSS receivers reported in Table 11 (2.007 and 0.700 m) proved to be better than the accuracy estimated in Bandini et al. [7] and more in accordance with Bogoyavlensky et al. [10]. It seems improper to define the Deeper Smart Sonar internal GNSS receiver as “highly accurate” as in Giambastiani et al. [9]. However, it proved to have good accuracy. The ΔV values reported in Table 13 (between 0.01 and 0.04 m) showed accuracy in measuring depth in shallow water better than the accuracy estimated in Kellerer-Pirklbauer et al. [11] and more in accordance with Bandini et al. [7]. The differences and similarities found may depend on the different measurement methods used and the technological advancement of the sensors studied. The μ 2D values of the G > S > P Sys in PPK positioning reported in Tables 11 and 12 (0.043 and 0.037 m) proved that the G > S > P Sys is more accurate than the method presented in Bandini et al. [7] and logistically not strictly dependent on the use of a UAV. Compared to the system proposed in Bandini et al. [16], the G > S > P Sys allows excellent real-time geolocation in SPP compatible with the THU value of the Exclusive Order. Furthermore, the synchronisation principle of the G > S > P Sys is potentially applicable to other sensors (e.g., optical sensors) that use the smartphone for geolocation. The implementation of sensors via smartphones had the advantage of prototyping and operating the system easily, and quickly and saving microchips during the semiconductor crisis. In addition, as the system is lightweight, it can also be moved by UAVs and USVs [41]. However, it must be considered that the system

proposed in Bandini et al. [16] managed multiple devices and an intrinsic weakness of a system developed on smartphones is that it is vulnerable to malfunctions due to the different types of smartphone models and the updates that operating systems and apps will receive during the time.

Concerning the 3D modelling of natural surfaces, analysing the C2M values in Table 14, it can be seen that the 3D model FCR obtained the best μ 3D value. On the other hand, the values of σ 3D differ marginally. Observing the values of the 3D model of artificial structure, the $G > S > P$ Sys and the proposed 3D modelling pipeline proved to be able to achieve centimetric accuracy and precision values.

Particularly interesting is the analysis of interpolation by ML. Comparing the bathymetric grids in Figure 6 and the 3D models in Figure 7, it can be seen that the grid FCR preserved the general formal layout of the grid IDW but punctually tried to correct the values, according to the sonar points used as training features. As can be seen in Figure 15c, this made the 3D model FCR section numerically similar to the 3D model OK section.

Finally, to give the reader a more complete view, a comparison was performed between the proposed spacetime PPK synchronisation method and another possible time-only PPK synchronisation method. In time-only PPK synchronisation, the sonar time was synchronised in post-processing directly with the GPS Time of the File PPK (for the synchronisation the times were converted to a common Coordinated Universal Time—UTC format). This method not requiring any intermediate steps (there is no previous electronic and spatial synchronisation), but produces a natural error due to the synchronisation of two different clocks with two different times (the sonar clock and the GPS clock) and only allows synchronisation up to the second. The performances obtained with this method were a μ 2D of 0.308 m, a σ 2D of 0.130 m and a THU of 0.318 m. The performances are lower than the spatio-temporal PPK synchronisation method proposed. However, they are compatible with the THU values of the Exclusive Order.

5. Conclusions

In this paper, smart low-cost sensors implementable via smartphones were used in order to obtain bathymetric data and an original method for 3D modelling of natural and artificial underwater environments was developed.

The main topics addressed in this research were:

1. Evaluation via analytical tests of the performance of the Deeper Smart Sonars CHIRP+ and Pro+ 2 in surveys conducted in shallow water;
2. Development and experimentation of a system to synchronise the Deeper Smart Sonars with an external GNSS receiver via smartphone to improve sonar geolocation in real-time and post-processing;
3. Experimentation of a mapping method based on an ML approach;
4. Implementation of a pipeline for 3D modelling of underwater natural surfaces and artificial structures.

Based on the results obtained, it is possible to deduce that Deeper Smart Sonars are excellent sensors for conducting surveys in natural aquatic environments, characterized by regular seabed for scientific applications, e.g., in biology, geology, climatology, etc. In the case of surveys of artificial structures underwater, detailed surveys of natural environments close to the coast and/or with a complex bottom, or in the case of data fusion between aquatic and terrestrial environments, it would be preferable to use the $G > S > P$ Sys with spacetime PPK synchronisation to achieve better performances in the geolocation of bathymetric data and in the subsequent 3D modelling.

In this case study, the ML based mapping method proved to be able to achieve comparable if not superior results to established interpolation methods. An advantage of ML mapping is the automaticity of the method compared to the classical geostatistical methods. In future research, further studies will be conducted, e.g., varying the morphology and nature of the surface to be interpolated, in order to accumulate further data in different scenarios.

The proposed 3D modelling pipeline has proven to be flexible, easily implemented, and capable of producing models with centimetric accuracy and precision. The opportunity to import bathymetric data into MeshLab and Rhinoceros[®] 7 allows 3D modelling by various algorithms depending on the goals. Furthermore, the import into CloudCompare can allow the geometric analysis of data via eigenfeatures analysis [42]. Finally, it is believed that the modelling of sonar data in specific software, such as CloudCompare, MeshLab and Rhinoceros[®] 7, would allow in future research an easier approach to data fusion collected with different techniques (photogrammetry, Light Detection And Ranging—LiDAR, etc.) and in different environments (water, ground, etc.)

Author Contributions: Conceptualization, G.V., D.C., M.P. and V.S.A.; methodology, G.V., D.C., M.P. and V.S.A.; software, G.V., D.C., M.P. and V.S.A.; validation, G.V., D.C., M.P. and V.S.A.; formal analysis, G.V., D.C., M.P. and V.S.A.; investigation, G.V., D.C., M.P. and V.S.A.; resources, G.V., D.C., M.P. and V.S.A.; data curation, G.V., D.C., M.P. and V.S.A.; writing—original draft preparation, G.V., D.C., M.P. and V.S.A.; writing—review and editing, G.V., D.C., M.P. and V.S.A.; visualization, G.V., D.C., M.P. and V.S.A. All authors have read and agreed to the published version of the manuscript.

Funding: This research received no external funding.

Institutional Review Board Statement: Not applicable.

Informed Consent Statement: Not applicable.

Data Availability Statement: Not applicable.

Conflicts of Interest: The authors declare no conflict of interest.

Appendix A

Figures A1 and A2 show the real-time planimetric static SPP accuracy of the Deeper Smart Sonar CHIRP+ and the Deeper Smart Sonar Pro+ 2 during an observation time of 3600 s (1 h).

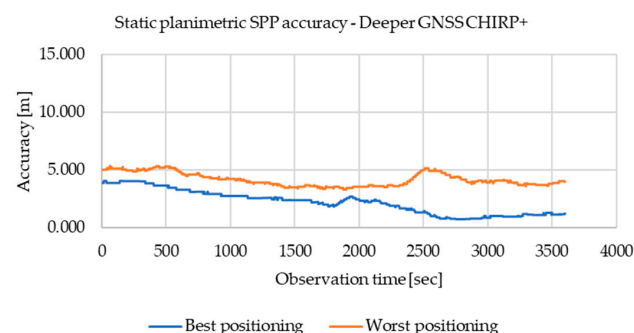


Figure A1. Accuracy (best and worst) in real-time planimetric static SPP of the Deeper Smart Sonar CHIRP+ during 3600 s.

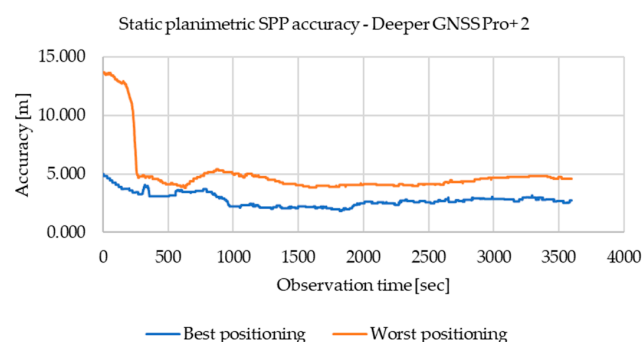


Figure A2. Accuracy (best and worst) in real-time planimetric static SPP of the Deeper Smart Sonar Pro+ 2 during 3600 s.

Figure A3 shows the Signal-to-Noise Ratio of the Huawei P30 Pro for L1 and L5 in the best and worst positioning obtained in 3600 s during 8 h of observation.

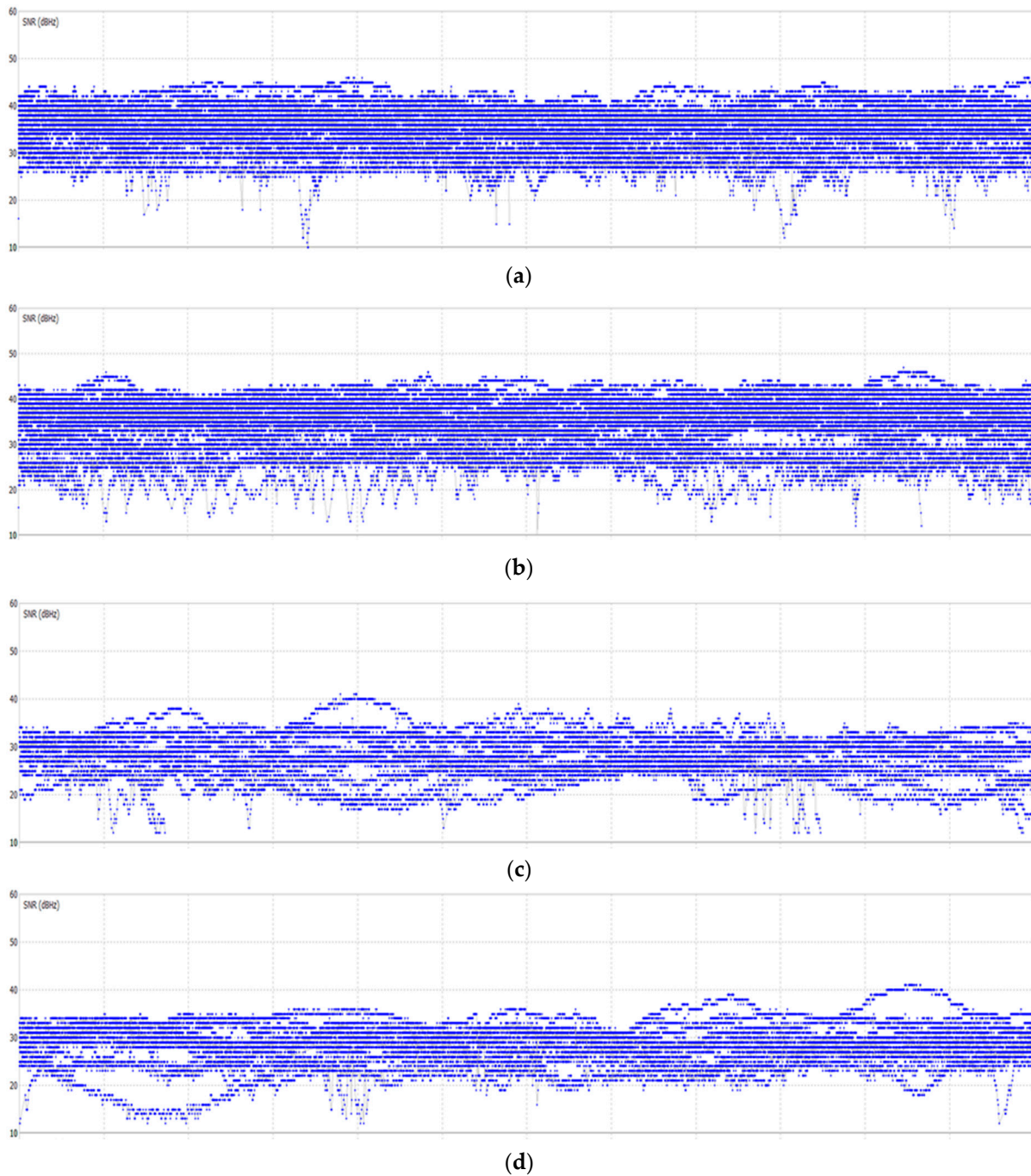


Figure A3. For the Huawei P30 Pro: (a) best SNR for L1; (b) worst SNR for L1; (c) best SNR for L5; (d) worst SNR for L5.

Figure A4 shows a diagram representing the evolution of the accuracy in 3D static post-processing positioning of the $G > S > P$ Sys during 3600 s. In grey are represented the data post-processed in static mode and in yellow the data post-processed in PPP mode. The accuracy was calculated using the following formula:

$$\Delta 3D = \sqrt{\Delta E^2 + \Delta N^2 + \Delta U^2} \tag{A1}$$

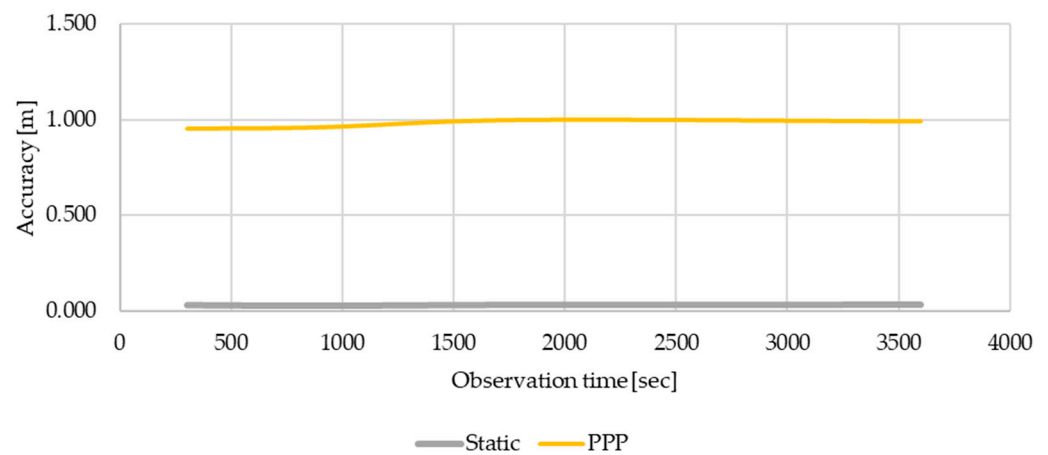


Figure A4. Accuracy in static 3D post-processed positioning in static mode (grey) and in PPP mode (yellow) of the G > S > P Sys.

Figure A5 shows a comparison between the G > S > P Sys and the Deeper Smart Sonar CHIRP+ and Pro+ 2 positioning data and the real trajectory travelled. The real trajectory is represented in green, the points surveyed in SPP by the G > S > P Sys are represented in red, the points processed in PPP by the G > S > P Sys are represented in orange and the points processed in PPK by the G > S > P Sys are represented in blue. The points surveyed by Deeper Smart Sonar CHIRP+ are represented in brown and the points surveyed by Deeper Smart Sonar Pro+ 2 are represented in magenta.

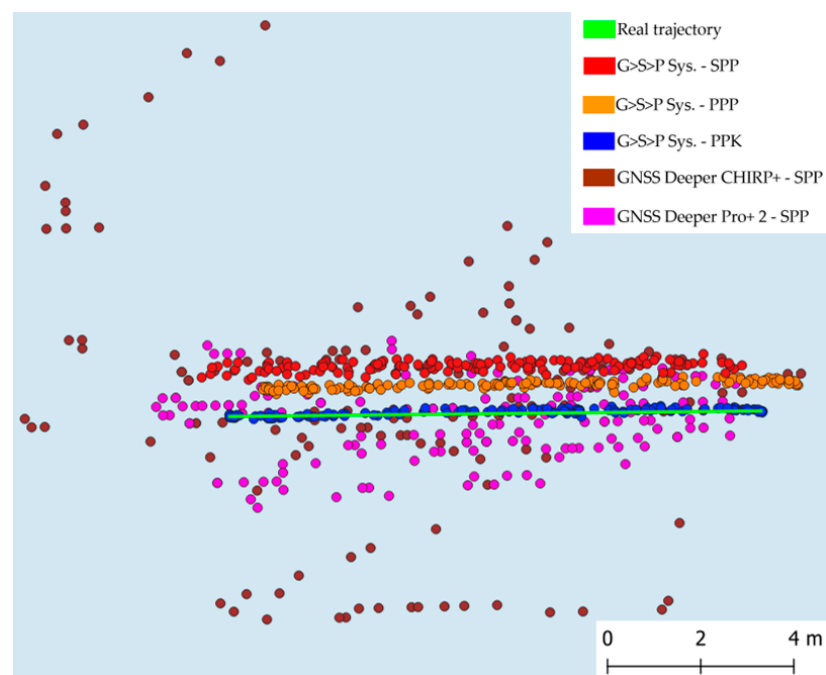


Figure A5. Comparison between the positionings of the G > S > P Sys and the Deeper Smart Sonars compared to the real trajectory in the sea test.

Figure A6 shows the histograms of the C2M analysis carried out on the pool (Figure A6a) and on the bottom of the pool (Figure A6b).

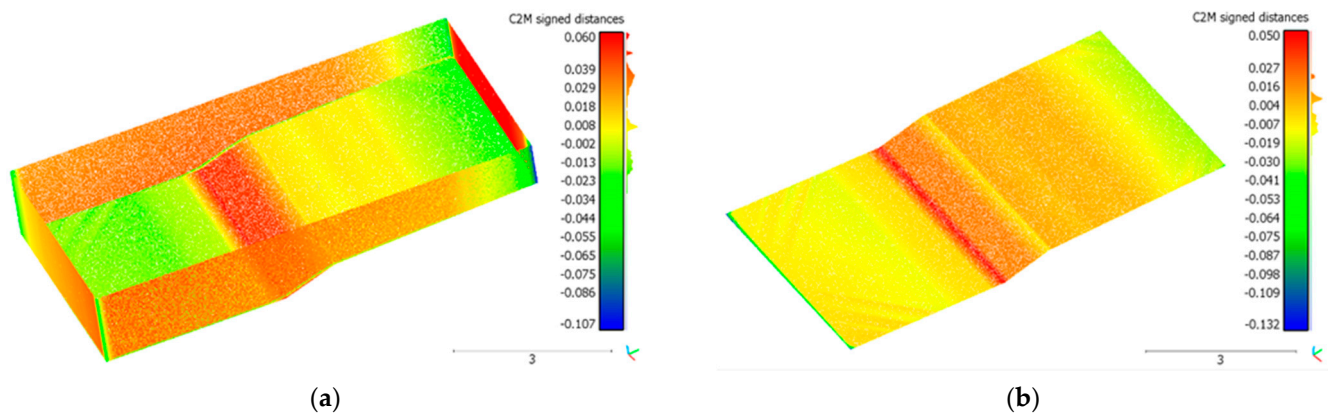


Figure A6. Histograms of the C2M analysis performed on the pool (a) and on the pool bottom (b).

References

- Cormier, R.; Elliott, M. SMART Marine Goals, Targets and Management—Is SDG 14 Operational or Aspirational, Is ‘Life Below Water’ Sinking or Swimming? *Mar. Pollut. Bull.* **2017**, *123*, 28–33. [[CrossRef](#)] [[PubMed](#)]
- Ryabinin, V.; Barbière, J.; Haugan, P.; Kullenberg, G.; Smith, N.; McLean, C.; Troisi, A.; Fischer, A.; Aricò, S.; Aarup, T.; et al. The UN Decade of Ocean Science for Sustainable Development. *Front. Mar. Sci.* **2019**, *6*, 10. [[CrossRef](#)]
- Helminen, J.; Linnansaari, T.; Bruce, M.; Dolson-Edge, R.; Curry, R.A. Accuracy and Precision of Low-Cost Echosounder and Automated Data Processing Software for Habitat Mapping in a Large River. *Diversity* **2019**, *11*, 116. [[CrossRef](#)]
- Tonion, F.; Pirotti, F.; Faina, G.; Paltrinieri, D. A MACHINE LEARNING APPROACH TO MULTISPECTRAL SATELLITE DERIVED BATHYMETRY. *ISPRS Ann. Photogramm. Remote Sens. Spat. Inf. Sci.* **2020**, *3*, 565–570. [[CrossRef](#)]
- Bio, A.; Gonçalves, J.A.; Magalhães, A.; Pinheiro, J.; Bastos, L. Combining Low-Cost Sonar and High-Precision Global Navigation Satellite System for Shallow Water Bathymetry. *Estuaries Coasts* **2022**, *45*, 1000–1011. [[CrossRef](#)]
- Monteys, X.; Harris, P.; Caloca, S.; Cahalane, C. Spatial Prediction of Coastal Bathymetry Based on Multispectral Satellite Imagery and Multibeam Data. *Remote Sens.* **2015**, *7*, 13782–13806. [[CrossRef](#)]
- Bandini, F.; Olesen, D.; Jakobsen, J.; Kittel, C.M.M.; Wang, S.; Garcia, M.; Bauer-Gottwein, P. Technical Note: Bathymetry Observations of Inland Water Bodies Using a Tethered Single-Beam Sonar Controlled by an Unmanned Aerial Vehicle. *Hydrol. Earth Syst. Sci.* **2018**, *22*, 4165–4181. [[CrossRef](#)]
- Alvarez, L.V.; Moreno, H.A.; Segales, A.R.; Pham, T.G.; Pillar-Little, E.A.; Chilson, P.B. Merging Unmanned Aerial Systems (UAS) Imagery and Echo Soundings with an Adaptive Sampling Technique for Bathymetric Surveys. *Remote Sens.* **2018**, *10*, 1362. [[CrossRef](#)]
- Giambastiani, Y.; Giusti, R.; Cecchi, S.; Palomba, F.; Manetti, F.; Romanelli, S.; Bottai, L. Volume Estimation of Lakes and Reservoirs Based on Aquatic Drone Surveys: The Case Study of Tuscany, Italy. *J. Water Land Dev.* **2020**, *VII–IX*, 84–96. [[CrossRef](#)]
- Bogoyavlensky, V.; Bogoyavlensky, I.; Nikonov, R.; Kishankov, A. Complex of Geophysical Studies of the Seyakha Catastrophic Gas Blowout Crater on the Yamal Peninsula, Russian Arctic. *Geosciences* **2020**, *10*, 215. [[CrossRef](#)]
- Kellerer-Pirklbauer, A.; Avian, M.; Benn, D.I.; Bernsteiner, F.; Krisch, P.; Ziesler, C. Buoyant Calving and Ice-Contact Lake Evolution at Pasterze Glacier (Austria) in the Period 1998–2019. *Cryosphere* **2021**, *15*, 1237–1258. [[CrossRef](#)]
- Broere, S.; van Emmerik, T.; González Fernández, D.; Luxemburg, W.; de Schipper, M.; Cózar Cabañas, A.; van de Giesen, N. Towards Underwater Macroplastic Monitoring Using Echo Sounding. *Front. Earth Sci.* **2021**, *9*, 628704. [[CrossRef](#)]
- Ruffell, A.; Lally, A.; Rocke, B. Dronar—Geoforensic Search Sonar from a Drone. *Forensic Sci.* **2021**, *1*, 202–212. [[CrossRef](#)]
- Sanjou, M.; Kato, K.; Aizawa, W.; Okamoto, T. Development of Drone-Type Float for Surface-Velocity Measurement in Rivers. *Env. Fluid Mech* **2022**, *22*, 955–969. [[CrossRef](#)]
- Koutalakis, P.; Zaimis, G.N. River Flow Measurements Utilizing UAV-Based Surface Velocimetry and Bathymetry Coupled with Sonar. *Hydrology* **2022**, *9*, 148. [[CrossRef](#)]
- Bandini, F.; Kooij, L.; Mortensen, B.K.; Caspersen, M.B.; Thomsen, L.G.; Olesen, D.; Bauer-Gottwein, P. Mapping Inland Water Bathymetry with Ground Penetrating Radar (GPR) on Board Unmanned Aerial Systems (UASs). *J. Hydrol.* **2023**, *616*, 128789. [[CrossRef](#)]
- International Hydrographic Organization. *IHO Standards for Hydrographic Surveys*, 6th ed.; Special Publication No. 44; International Hydrographic Organization: Monte Carlo, Monaco, 2020.
- Costantino, D.; Voza, G.; Alfio, V.S.; Pepe, M. Strategies for 3D Modelling of Buildings from Airborne Laser Scanner and Photogrammetric Data Based on Free-Form and Model-Driven Methods: The Case Study of the Old Town Centre of Bordeaux (France). *Appl. Sci.* **2021**, *11*, 10993. [[CrossRef](#)]
- Breiman, L. Random Forests. *Mach. Learn.* **2001**, *45*, 5–32. [[CrossRef](#)]
- Pereira, G.W.; Valente, D.S.M.; de Queiroz, D.M.; Santos, N.T.; Fernandes-Filho, E.I. Soil Mapping for Precision Agriculture Using Support Vector Machines Combined with Inverse Distance Weighting. *Precis. Agric.* **2022**, *23*, 1189–1204. [[CrossRef](#)]

21. Pereira, G.W.; Valente, D.S.M.; Queiroz, D.M.d.; Coelho, A.L.d.F.; Costa, M.M.; Grift, T. Smart-Map: An Open-Source QGIS Plugin for Digital Mapping Using Machine Learning Techniques and Ordinary Kriging. *Agronomy* **2022**, *12*, 1350. [CrossRef]
22. Ferreira, I.O.; Rodrigues, D.D.; dos Santos, G.R.; Rosa, L.M.F. IN BATHYMETRIC SURFACES: IDW OR KRIGING? *Bol. Ciênc. Geod.* **2017**, *23*, 493–508. [CrossRef]
23. Parente, C.; Vallario, A. Interpolation of Single Beam Echo Sounder Data for 3D Bathymetric Model. *IJACSA* **2019**, *10*, 6–13. [CrossRef]
24. Matheron, G. *Traité de Géostatistique Appliquée*; Editions Technip: Paris, France, 1962.
25. Posa, D.; De Iaco, S. *Geostatistica: Teoria e Applicazioni*; Giappichelli: Turin, Italy, 2009.
26. Alcaras, E.; Carnevale, L.; Parente, C. Interpolating Single-Beam Data for Sea Bottom GIS Modelling. *Int. J. Emerg. Trends Eng. Res* **2020**, *8*, 591–597. [CrossRef]
27. Kazhdan, M.; Bolitho, M.; Hoppe, H. Poisson Surface Reconstruction. In Proceedings of the Fourth Eurographics Symposium on Geometry Processing, Cagliari, Italy, 26–28 June 2006; Volume 7.
28. Kazhdan, M.; Hoppe, H. Screened Poisson Surface Reconstruction. *ACM Trans. Graph. (ToG)* **2013**, *32*, 1–13. [CrossRef]
29. Jones, E.J.W. *Marine Geophysics*; John Wiley & Sons Inc.: Hoboken, NJ, USA, 1999; ISBN 978-0-471-98694-2.
30. Lurton, X. *An Introduction to Underwater Acoustics: Principles and Applications*; Springer: Berlin/Heidelberg, Germany, 2002; Volume 2.
31. Semler, Q.; Mangin, L.; Moussaoui, A.; Semin, E. DEVELOPMENT OF A LOW-COST CENTIMETRIC GNSS POSITIONING SOLUTION FOR ANDROID APPLICATIONS. In *International Archives of the Photogrammetry, Remote Sensing & Spatial Information Sciences*; EBSCO: Ipswich, MA, USA, 2019.
32. Takasu, T.; Yasuda, A. Development of the Low-Cost RTK-GPS Receiver with an Open Source Program Package RTKLIB. In *International Symposium on GPS/GNSS*; International Convention Center Jeju Korea: Seogwipo-si, Republic of Korea, 2009; Volume 1.
33. Rtklibexplorer Rtklibexplorer (Rtklibexplorer)/Repositories GitHub. Available online: <https://github.com/rtklibexplorer?tab=repositories> (accessed on 8 January 2023).
34. Jivthesh, M.R.; Gaushik, M.R.; Shibu, N.B.S.; Raj, D.; Rao, S.N. A Comprehensive Survey of Web and Mobile Apps for Fishermen. In *Proceedings of the Data, Engineering and Applications*; Sharma, S., Peng, S.-L., Agrawal, J., Shukla, R.K., Le, D.-N., Eds.; Springer Nature: Singapore, 2022; pp. 199–211.
35. Tétéault, P.; Kouba, J.; Héroux, P.; Legree, P. CSRS-PPP: An Internet Service for GPS User Access to the Canadian Spatial Reference Frame. *Geomatica* **2005**, *59*, 17–28. [CrossRef]
36. Pepe, M.; Costantino, D.; Vozza, G.; Alfio, V.S. Comparison of Two Approaches to GNSS Positioning Using Code Pseudoranges Generated by Smartphone Device. *Appl. Sci.* **2021**, *11*, 4787. [CrossRef]
37. Cardellicchio, N.; Annicchiarico, C.; Di Leo, A.; Giandomenico, S.; Spada, L. The Mar Piccolo of Taranto: An Interesting Marine Ecosystem for the Environmental Problems Studies. *Environ. Sci. Pollut. Res.* **2016**, *23*, 12495–12501. [CrossRef]
38. Di Leo, A.; Annicchiarico, C.; Cardellicchio, N.; Giandomenico, S.; Conversano, M.; Castellano, G.; Basile, F.; Martinelli, W.; Scortichini, G.; Spada, L. Monitoring of PCDD/Fs and Dioxin-like PCBs and Seasonal Variations in Mussels from the Mar Grande and the Mar Piccolo of Taranto (Ionian Sea, Southern Italy). *Environ. Sci. Pollut. Res.* **2014**, *21*, 13196–13207. [CrossRef]
39. Girardeau-Montaut, D. *CloudCompare*; EDF R&D Telecom ParisTech: Paris, France, 2016.
40. Cignoni, P.; Callieri, M.; Corsini, M.; Dellepiane, M.; Ganovelli, F.; Ranzuglia, G. Meshlab: An Open-Source Mesh Processing Tool. In Proceedings of the Eurographics Italian Chapter Conference, Salerno, Italy, 2–4 July 2008; Volume 2008, pp. 129–136.
41. Pepe, M.; Alfio, V.S.; Costantino, D. UAV Platforms and the SfM-MVS Approach in the 3D Surveys and Modelling: A Review in the Cultural Heritage Field. *Appl. Sci.* **2022**, *12*, 12886. [CrossRef]
42. Costantino, D.; Vozza, G.; Pepe, M.; Alfio, V.S. Smartphone LiDAR Technologies for Surveying and Reality Modelling in Urban Scenarios: Evaluation Methods, Performance and Challenges. *Appl. Syst. Innov.* **2022**, *5*, 63. [CrossRef]

Disclaimer/Publisher’s Note: The statements, opinions and data contained in all publications are solely those of the individual author(s) and contributor(s) and not of MDPI and/or the editor(s). MDPI and/or the editor(s) disclaim responsibility for any injury to people or property resulting from any ideas, methods, instructions or products referred to in the content.